Eberhard Karls Universität Tübingen
Fakultät für Informations- und Kognitionswissenschaften
Wilhelm-Schickard-Institut für Informatik

Diplom Thesis Bioinformatics

# Wide Field of View Head Mounted Display: Integration and Evaluation in a Motion Simulator

Volker Grabe

01.06.2010

**Advisor**

Dr. Paolo Robuffo Giordano
Computer Science Engineering
Human Perception, Cognition and Action
Max Planck Institute for Biological Cybernetics

**Referees**

Prof. Dr. Wolfgang Rosenstiel
Computer Science
Wilhelm-Schickard-Institut für Informatik
Universität Tübingen

Prof. Dr. Heinrich H. Bülthoff
Biology
Human Perception, Cognition and Action
Max Planck Institute for Biological Cybernetics

**Grabe, Volker:**
*Wide Field of View Head Mounted Display:*
*Integration and Evaluation in a Motion Simulator*
Diplom Thesis Bioinformatics
Eberhard Karls Universität Tübingen
Thesis period: June 2009 - May 2010

## Abstract

Head Mounted Displays (HMDs) are a flexible and small-sized alternative to projection screens as a visualization device on motion simulators. However, only few HMDs on the market feature a wide field of view (FoV) combined with a low weight. Among these, the xSight 6123 HMD from Sensics, with a horizontal FoV of 118° and a weight of 400 g, is a particularly suitable choice for use on a motion simulator.

In this work, we integrated the xSight 6123 HMD into the virtual reality setup of our CyberMotion simulator. Therefore, we developed a new camera class for visual systems with stereo capabilities for the open source 3D engine OGRE. Furthermore, we investigated the benefit of the HMD compared to a projection screen by designing and conducting experiments on flight control tasks and driving simulation. We found that subjects show a better control performance when a screen is used, and that a narrow FoV does not affect their performance. Therefore, we conclude that on motion simulators, whenever possible, a projection system should be preferred to an HMD.

## Acknowledgements

During the last year, I had the chance to meet many exceptional people. All of them contributed and influenced my work in some way. I like to thank all of them, especially my advisor Paolo Robuffo Giordano for guiding my work with many improving suggestions as well as Paolo Pretto who supervised the final experiment on driving simulators and the resulting publication.

I am grateful to Professor Heinrich H. Bülthoff for giving me the chance to write this thesis in his department and providing many helpful inputs, and to Professor Wolfgang Rosenstiel for the intensive support in many means not only during the last year. Betty Mohler and Joachim Tesch helped with their expertise in virtual reality, head mounted displays and image generation. Furthermore, they restocked my chocolate chip supply with every trip to the USA for which I cannot thank enough. Tobias Meilinger gave me insights in the design of psychophysical experiments. Harald Teufel and Michael Kerger introduced me to the programming and operation of the simulator. Together with Karl Beykirch they were very patient and helpful during preparation and conduction of my experiments and even worked overtime.

Paolo Robuffo Giordano, Agnes Meyder, Katharina Mülling, Betty Mohler and Trevor Dodds offered their time to review this thesis! Thanks a lot for your great help!

Furthermore, I like to thank all of my 15 subjects. Some of them had a hard time suffering from motion sickness and I honor their decision to help me anyway. Special thanks goes to Hendrik Deusch, Carlo Masone, Christian Neth, Johannes Stephan and Oliver Krömer who agreed to help as test subjects prior to the experiments without any reward. This work would not have been possible without any of them.

Finally, I like to thank my parents for the financial support during the last six years and my friends who supported me throughout my time at the university or even longer during good and bad times. Last, I like to thank Katharina Mülling for just being present in my life.

# Contents

# List of Figures

# List of Tables

# List of Abbreviations

| | |
|---|---|
| **API** | Application Programming Interface |
| **AMST** | AMST Systemtechnik GmbH |
| **ANOVA** | ANalysis Of VAriance |
| **CAN-Bus** | Controller Area Network Bus |
| **DLR** | Deutsches zentrum für Luft- und Raumfahrt (German Aerospace Center) |
| **DVI** | Digital Visual Interface |
| **DoF / DoFs** | Degree of Freedom / Degrees of Freedom |
| **EDID** | Extended Display Identification Data |
| **FoV** | Field of View |
| **FPGA** | Field-Programmable Gate Array |
| **GFDL** | GNU Free Documentation License |
| **GNU** | GNU's Not Unix |
| **HMD** | Head Mounted Display |
| **IR** | InfraRed |
| **LCoS** | Liquid Crystal on Silicon |
| **LED** | Light Emitting Diode |
| **MPI** | Max-Planck-Institute |
| **NASA** | National Aeronautics and Space Administration |
| **OGRE** | Object-Oriented Graphics Rendering Engine |
| **OLED** | Organic Light Emitting Diode |
| **PC** | Personal Computer |
| **px** | PiXel |
| **RMS / RMSE** | Root Mean Square / Root Mean Square Error |
| **UDP** | User Datagram Protocol |
| **USB** | Universal Serial Bus |
| **TCP/IP** | Transmission Control Protocol/Internet Protocol |
| **TNO** | nederlandse organisatie voor Toegepast Natuurwetenschappelijk Onderzoek (Netherlands Organisation for Applied Scientific Research) |
| **VR** | Virtual Reality |

# Introduction

For a long time, the diagonal field of view (FoV) of most commercially available HMDs was about 60° and thus very narrow, causing discomfort in the user [Mon-Williams et al., 1993]. Furthermore, HMDs could not be used in situations that required fast and precise action since the user had to compensate for the small FoV with additional head rotations. Apart from the FoV, a weight of more than 1 kg would have caused severe neck strain and made HMDs unsuitable for use on a motion simulator with high accelerations.

Since many simulators lack the space for large projection systems, light weight HMDs with a wide FoV would be a serious alternative. Recently, Sensics launched its xSight series of HMDs. They offer a horizontal FoV of up to 118° at a weight of 400 g. HMDs with a wide FoV are known to reduce the users discomfort [Peli, 1998], and thus are a potentially valuable choice in research applications on motion simulators.

The Max Planck Institute (MPI) for Biological Cybernetics decided to purchase the xSight HMD with the largest FoV available for virtual reality applications. As part of this thesis, we integrated this HMD into our motion simulator for comparison with commonly used projection screens. Additionally, we tested the influence of the visual device and the FoV on the performance in vehicle control tasks typically performed on motion simulators in research.

## Goal of the Thesis

This thesis addresses the following topics:

**Integration of the Sensics xSight HMD into a Virtual Environment.** Apart from the organization of the necessary computational equipment, it is necessary to implement a new camera class that is able to generate a video stream for both eyes synchronously. Therefore, all parameters of the two virtual cameras according to the design of the HMD with a partial binocular overlap and an asymmetric FoV have to be identified and determined.

**Installation of the HMD on the CyberMotion Simulator.** The HMD has to be installed on the simulator with respect to the special constrains given by the hardware that powers the HMD. Cable length is limited for the connection between the different components but the fragile electronic system has to be protected from high accelerations on the simulator. On the computational side, this issue involves the design and implementation of a protocol for the communication between the PCs controlling simulator and vision.

**Design, Implementation, Conduction and Evaluation of an Experiment.** In order to test the enhancement of the CyberMotion simulator through the HMD, an experiment has

to be designed. The final part of the thesis will be the implementation of the resulting simulator behavior, conduction of the experiment and evaluation of the results.

## Organization of the Thesis

In Chapter 1, background information on the biological aspects of motion simulators will be provided, especially on how humans perceive motion and visual stimuli. We will then present existing motion simulators and devices to provide visual feedback.

Chapter 2 will give an in-depth introduction to the CyberMotion simulator at the MPI for Biological Cybernetics. The HMD used in this work is described in Chapter 3. These chapters provide both technical information on the two devices as well as on their software environment.

In Chapter 4, we will summarize the experiments carried out with the HMD on the CyberMotion simulator. Therefore we will first line out several preliminary tests on the influence of the FoV size on performance in flight control tasks. These tests were carried out only with the existing projection system. Since no influence was measurable, we will afterwards present a study on the comparison of HMDs and screens on the CyberMotion simulator. This study was accepted as a contributed paper for the Driving Simulation Conference 2010 in Paris, France [Grabe et al., 2010].

Finally, Chapter 5 will summarize the results of the thesis by drawing conclusions and illustrating open points and future directions.

# Chapter 1

# Background Information

Motion simulators are used to create a virtual world with realistic motion cues around a human. In particular, they try to stimulate the visual and vestibular sense as accurately as possible. The virtual world can be perceived vestibularly through the simulator and is presented visually on a display device. Both together are commonly referred to as the virtual reality setup 'Motion Simulator'.

In oder to understand the underlying concepts of motion simulators, one has to gain a basic knowledge on how humans perceive and process sensory information. Section 1.1 will give an overview on visual and vestibular information processing as the most important topics in biology for motion simulators. The last two sections introduce different state of the art simulator technologies and visualization devices used today. Applications for theses systems will also be presented.

## 1.1 Biologigal Aspects of Motion Simulators

Optical motion perception, called 'Vection', interacts closely with the vestibular system not only for a precise self-localization of the human body. To keep an image stabilized on the retina, the vestibulo-ocular reflex, one of the fastest in the human body, controls the eye movement when the head is rotated. Together with the proprioceptive sense, the two senses allow us to maintain the orientation of our body relative to the surrounding environment. This ability is known as 'Spatial Orientation'. However, in certain situations the visual and vestibular senses can be in conflict. These situations cause severe sickness in many humans.

### 1.1.1 Optical Sensing and Information Processing

Vision is the predominant sense in humans [Ishida et al., 2008; Wright et al., 2005]. Consequently, the eye has been intensively studied for many years and is well understood.

The eye transforms electro magnetic waves into neuronal impulses. The light enters the eye through the cornea, is focused by the lens, passes through the liquid filled eye ball and eventually reaches the retina (Figure 1.1a). The retina on the back of the eye holds sensory cells of two types: cones and rods. Cones are concentrated in the fovea, show a short reaction time and a high resolution. Three different types of cones, of which each is sensitive to one specific wave

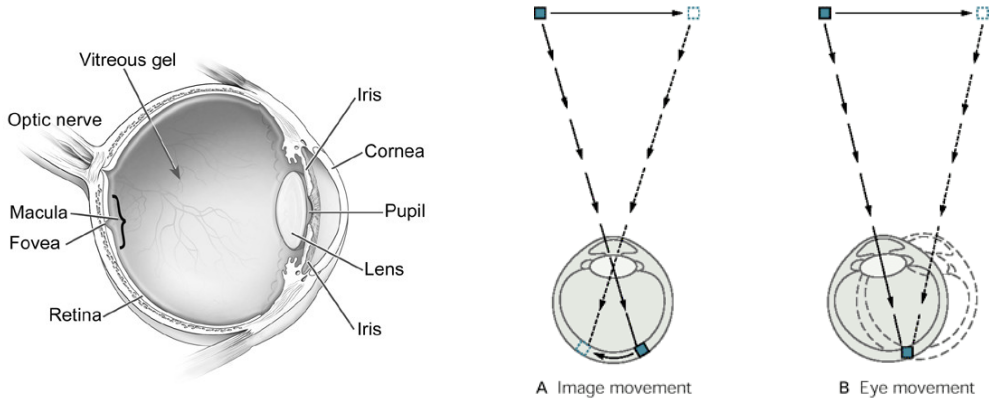


**Figure 1.1:** From left to right: (a) Diagram of the right human eye cut in the horizontal plane. Picture taken from `http://www.nei.nih.gov/`. (b) Two ways of local motion perception. A: The projection of the object moves on the retina. B: The object is projected to the same location while the eye follows the object. Picture taken from [Kandel et al., 2000].

length, are responsible for color perception. Rods are found in the periphery of the retina. They are more sensitive to low light conditions (even single photons can be detected) and therefore specialized for night vision. However, they only allow achromatic light perception [Kandel et al., 2000].

The information processing starts in the retina. Two layers of cells are connected in a grid shaped pattern directly to the sensory cells. The information from 125 million cones and rods is compressed to 1 million neurons which form the optic nerve [Kandel et al., 2000].

The human eye is able to detect light in a FoV of up to 90° lateral (horizontally to the side), 60° nasal (towards the nose), 60° superior (up) and 70° inferior (down). The FoV of binocular overlap and therefore stereo vision can range to 120°. The FoV for full color vision is approximately half as large in all dimensions [Axenfeld and Pau, 1992]. The resolution was shown to be in the range of 0.005° to 0.008° (depending on the measuring method) which corresponds to 150 to 200 pixels per degree [Westheimer, 2009].

The brain is able to detect local motion in two ways: 1. When an object moves, its projection moves over the retina while the eye is stationary. 2. The eye follows the movement and thus the image is projected to the same area on the retina. In the latter case, the brain calculates the speed from the rotation of the eye (Figure 1.1b). Both mechanisms act in combination [Kandel et al., 2000].

All objects visible to a viewer together with the surrounding background form the 'Optical Array'. Whenever only parts of this array move across the retina while the eye is stationary, the brain triggers a local movement of the object that is defined by the moving part of the array. If the largest portion of the optical array moves across the retina, self motion will be assumed. The pattern of this global 'Optical Flow' allows the brain to gain detailed information on the direction of movement. If the eyes are looking into the heading direction, optic flow will expand outward from a static point infinitely far away [Gibson, 1979; Goldstein, 2002]. Modulations of this pattern allow the sensation of additional rotations or sidewise motion. Furthermore, a moving observer has a certain range of depth perception since a close object moves further across the FoV than a far one. This cue is called 'Motion Parallax' [Ferris, 1972].

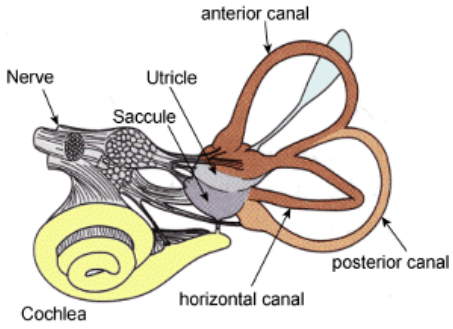


**Figure 1.2:** The vestibular system. Anterior, posterior and horizontal canal are used to perceive rotations of the head in space. The otoliths utricle and saccule are used to trigger translations. Picture published under GFDL.

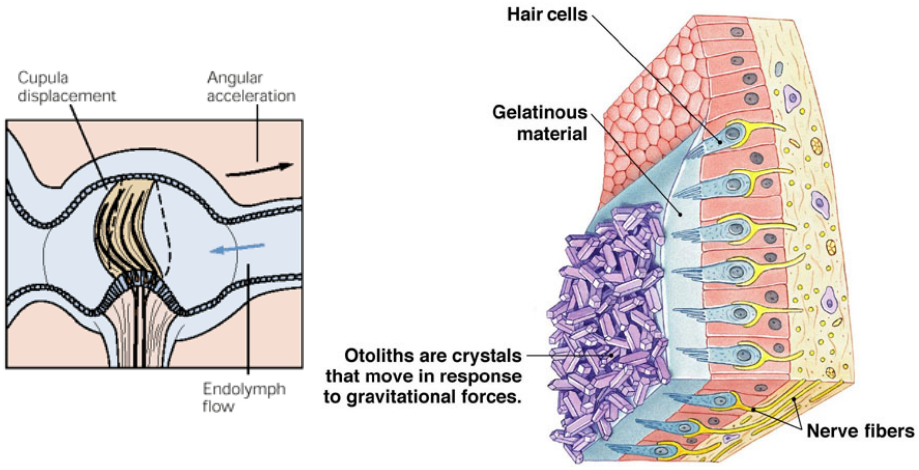


**Figure 1.3:** (a) Sensory system in the semicircular canals. Picture taken from [Kandel et al., 2000]. (b) Sensory system of utricle and saccule. Picture taken from Pearson Education.

### 1.1.2 Vestibular Sensing and Information Processing

The human vestibular system is located inside the inner ear. It consists of three semicircular canals and the two otolithic organs, saccule and utricle (Figure 1.2). Both systems are filled with endolymph.

Semicircular canals are responsible for the perception of rotations. Three canals form independent loops. One is located in the horizontal plane when the head is kept upright. The other two are positioned in a 45° angle relative to the midsagittal plane (it separates the head in a left and right half). This enables us to detect rotations in all three DoFs (Degrees of Freedom). If the head is moved, the liquid in the canals remains stationary due to its inertia. Thus, the walls of the canal move relatively to the lymph. A bundle of hair from hair cells stick into a gelatinous diaphragm called 'Cupula' at one end of each canal (Figure 1.3a). The flow of lymph displaces the cupula which induces a depolarization in the hair cells and thus an electronic impulse [Kandel et al., 2000].

Two sensory regions, saccule and utricle, are able to detect translational motion. The larger

utricle (3 mm) is in the horizontal plane of the upright head while the saccule has a vertical orientation. Both regions consist of many hair cells that extend into a gelatinous material that is covered with fine calcium carbonate particles, the 'Otoconia' (Figure 1.3b). Gravitational forces affect the otoconia, move the gelatinous material and therefore bend the hair cells which results in an electric signal. Since the hair cells are arranged in random pattern in both otolithic organs but each cell is only sensitive to motion in one dimension, saccule and utricle perceive motion in two dimensions. Both are oriented orthogonal to each other such that all three translational DoFs can be perceived [Kandel et al., 2000].

### 1.1.3 Motion Sickness

A sensory conflict between perceived visual and vestibular information causes sickness in most humans. It is believed that this behavior of the human body evolved in the past. At that time, a sensory conflict was most likely caused by a neurotoxin and thus regorgeing the toxin was a reasonable survival strategy [Treisman, 1977]. The special case of motion sickness caused by a simulator is also called 'Simulator Sickness'.

In general, three reasons may lead to motion sickness due to sensory conflicts. These reasons are:

**Motion is perceived mainly visually.** The conflict arises if the magnitude of perceived physical motion is smaller than the magnitude of visual motion. The conflict is strongest when no physical motion is present in stationary systems. This is the most common reason for motion sickness on simulators with a small workspace and when motion cueing is used. However, many young people are used to video games that present motion only visually and thus became accustomed to this type of conflict.

**Motion is perceived mainly vestibularly.** This conflict can be observed on a plane or ship. In these situations, the poor visual environment prevents a visual motion perception and motion is only perceived vestibularly. On a motion simulator, this conflict emerges when the end of the workspace is reached and the simulator breaks while a fluent motion is presented through the visual system .

**Visual and vestibular information are in contradiction.** On a motion simulator, this conflict can be perceived in centrifuges only and consideration is less important with most other system. The forces might not always match the visual perception since the observer is moving on a circular trajectory. This effect is known as 'Coriolis Effect'.

Motion sickness affects children more than adults. Furthermore, the occurrence and strength of symptoms varies between humans. However, the brain is able to adapt to perceptual conflicts after several hours of exposure, as seen with sailors [Reason, 1978]. The most common symptoms are:

- nausea, stomach awareness, burping, vomiting
- dizziness, difficulty focusing
- eyestrain

Based on the symptoms, several questionnaires were developed to measure simulator sickness [Kennedy et al., 1993]. We used a simplified version of Kennedy's questionnaire to exclude the data from subjects suffering from motion sickness.

To prevent simulator sickness, clear visual motion cues should be provided in the environment and vertical sinusoid motion should be avoided if possible. As a chemical treatment, transdermal patches, pills and chewing gums are commercially available. Chewing in general and the consumption of ginger are known as a natural therapy.

### 1.1.4 Psychophysical Methods

Psychophysics investigates the subjective perception of physical stimuli and forms a discipline within psychology. The main research instrument is a controlled experiment. Experiments are used to test opposing models or hypotheses against each other and to prove or disprove new theories. Control conditions are added to each experiment to ensure that the measured effect is only caused by the parameters varied throughout the experiment. This approach allows the elimination of external factors.

Depending on the research project, experiments can be designed in two ways. The most favored one is the 'Within Subject Design' were all subjects do the experiment under all conditions. In some cases this is not possible, as for studies that investigate the influence of age or gender on a specific task. In that case, the 'Between Subject Design' is chosen. Each condition is tested with one group of subjects and the results are compared between the groups. In a between subject design, more subjects have to be tested to reach the same statistical power as with a within subject design.

Statistical tests are used to test the influence of the investigated parameters against the control condition. If only one parameter was changed to one other condition and a normal distribution is assumed, a 'T-Test' can be used. To show an effect, one has to disprove the hypotheses that both control and varied condition show the same result. If a difference between the means of the collected data should be proved, a 'Double Ended T-Test' is used. In contrast, a 'Single Ended T-Test' is used to show that the mean is either larger or smaller than the one of the control condition. Different variations of the t-test can be used, depending on the underlying distribution. A 'Paired T-Test' is used, if the collected data is not pairwise independent, e.g. when one subject was tested on more than one condition in a within subject design. If more than two conditions have to be tested against each other, the 'Analysis of Variance' (ANOVA) provides a generalization of the t-test.

The result of a test is considered to be 'significant' if the result could have happened by chance with a probability of less than 5 %, based on the assumed distribution. If the probability is less than 1 %, the result is called 'highly significant'. The probability is often simply refered to as the '$p$-Value'. With an increasing number of subjects '$n$', the chance to obtain a result by chance drops and thus the significance increases.

The literature provides detailed background information on the design of experiments and the mathematical background [Bortz and Döring, 2006; Bortz, 2005].

## 1.2 Overview of Display Devices

In order to provide an immersive simulation, the presentation of high quality visual stimuli to the user is essential. Depending on the simulator technology, the availability and the desired experiment, there are several ways to provide visual feedback:

**Head Mounted Displays.** A HMD presents an image directly in front of the user's eyes on small screens. Since they are worn on the head, neither additional structures nor calibration after installation on the simulator are required. Stereo vision is possible without any additional equipment. Most HMDs are powered through an external box holding all necessary electronics. However, most HMDs weight at least 1 kg and the mass is centered on the forehead. In consequence, counter weights are unavoidable and add additional load. In order to effectively shield off the outside world, HMDs need to be worn tight, resulting in pressure on the skin and in some cases even claustrophobia. A selection of commercially available HMD solutions will be presented in Subsection 1.2.2.

**Small Screens on the Simulator.** The most common option to provide visual feedback on a motion simulator is a small projection screen on the motion platform in front of the seat. The screen is stationary relative to the subjects head. If a curved screen is used, additional hardware or special display drivers are needed to compensate for the curve. Back projection is used in advanced simulators if space permits. The projection screen used on the CyberMotion simulator is described in Subsection 1.2.1 in more detail.

**Large Projection Systems.** Opposed to a small screen that moves with the simulator, the simulator can be surrounded by one stationary large screen that covers all walls of the cave. A projection system of this type is expensive and sophisticated since several projectors have to overlap precisely to form one big image without any visual seams. Motion cueing is only feasible if a low latency synchronization between the motion simulator and the vision system is established and precise head tracking is available. The rendering power for a 360° projection requires a fast computer cluster or advanced view-dependent rendering algorithms [Xia and Varshney, 1996; Hoppe, 1997; Luebke and Erikson, 1997]. This solution is only feasible for simulators with a small motion range.

**Real Environments.** The most direct solution to provide visual feedback is to build a real environment around the simulator if the experiment does not require motion cueing. In that case, a synchronous simulation of physical and visual motion is possible. In most cases, it will be cheaper and faster to model an environment in virtual reality than to build a scenery around the simulator. Therefore, in research applications, a real environment is only feasible for abstract worlds (e.g. simple targets in an otherwise plane environment, Figure 1.4a).

### 1.2.1 MPI Projection Screen

The CyberMotion simulator at the MPI for Biological Cybernetics is equipped with a projection screen mounted in front of the seat with a horizontal FoV of 90° and a vertical FoV of 45°. A video projector displays an image of $1152 \times 450$ pixels on a curved screen at a distance of

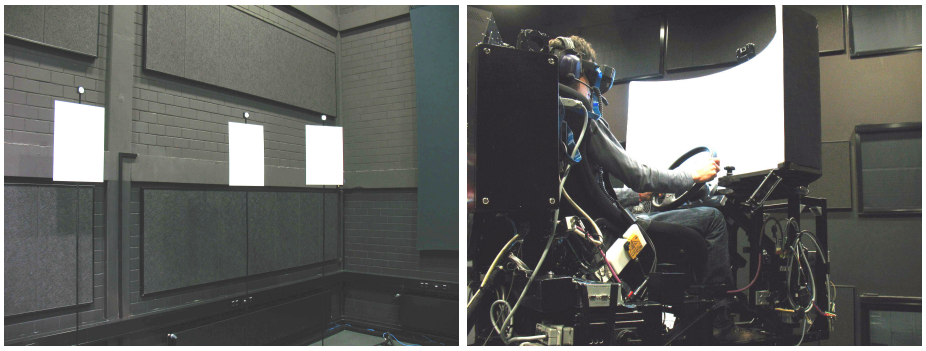

**Figure 1.4:** (a) Card board targets with a signal light on top form an abstract world around the motion simulator for side step maneuvers. (b) Projection system on the CyberMotion simulator.

approximately 73 cm in front of the subject's eyes (Figure 1.4b). A distortion compensator from eyevis GmbH is used to compensate for the curve in the surface of the screen. For the projection, a shock prove color laser projector was mounted on the left side of the seat. Optic fibers transmit the video signal from the vision PC in the control room onto the simulator.

### 1.2.2 Overview of recent HMD Solutions

HMDs are available in many configurations from different companies. To allow a quick overview, we loosely grouped them in three categories based on the covered FoV:

1. HMDs with a small diagonal FoV ($\leq 45°$),
2. HMDs with a medium FoV ($45° - 90°$) and
3. HMDs with a large FoV ($\geq 90°$)

Four HMDs from these categories are listed in Table 1.1 for comparison. Monocular or hand-held HMDs are not covered in this section since they are not suitable for the use on motion simulators.

HMDs of the first category are usually low cost devices for consumer markets. The best known product is the Z800 from eMagin (Table 1.1, Figure 1.5d). Two small OLED[1] displays present an image of $800 \times 600$ pixels in front of the user's eyes covering a diagonal FoV of 40° [eMagin Corporation, 2010]. No special effort was driven to shield off the surrounding world. The device weights only 230 g and features a build-in stereo head-set and an inertial head tracking system with six DoFs. Despite the the small FoV, the Z800 is used in research when several HMDs of the same kind are required under limited budget constraints.

Most research institutes use HMDs of the second category. The MPI operates the SX60 from nVis Inc. which offers a resolution of $1280 \times 1024$ pixels across a diagonal FoV of 60° [NVIS

[1] A **Organic Light Emitting Diode** is a light-emitting diode whose emissive electroluminescent layer is composed of a film of organic compounds. This layer of organic semiconductor material is formed between two electrodes, where at least one of the electrodes is transparent. OLED displays are light-emitting itself and thus do not require a backlight. However, blue colors wash out faster than red and green ones over the years.

Inc., 2010]. However, the employed LCoS[2] technology results in a weight of 1000 g. Since most of the weight is centered on the forehead, an additional counter weight on the back of the head is required. Thus, a system of this weight would cause sever neck strain under fast accelerations and therefore cannot be used on a motion simulator.

At the time of this work, only few HMDs of the third category were commercially available. The MPI owns the xSight 6123 from Sensics as part of a larger product family. nVis offers the model SX111 (Table 1.1, Figure 1.5a and b). The SX111 features a total FoV of 111° and a resolution of $1280 \times 1024$ pixels in each eye [NVIS Inc., 2010]. Since a similar LCoS chip was used for both SX60 and SX111 but the image is projected in different sizes, brightness and angular resolution are significantly worse in the SX111 compared to the SX60. The SX111 weights 1300 g not including a counter weight. We used a Sensics xSight 6123 with a horizontal FoV of 118° and a vertical FoV of 45° for our experiments [Sensics Inc., 2010]. The low weight of 400 g makes it particularly suitable for the use on a motion simulator. Each eye piece is rotated outwards off the viewing direction by 16.75° and consists of six individual OLED micro displays. Special lenses are used to overlap all six displays to one seamless image of $1920 \times 1200$ pixels in each eye. Given a binocular overlap of 63 % or 53°, the resolution of both eyes combined is approximatly $2664 \times 1200$ pixels.

All mentioned manufacturer tried to limit the weight of their HMDs and moved as many electronic components as possible into a separate control unit. However, the length of the connecting cables is fixed thus limiting the range of use. In most cases, the control unit would have to be mounted onto the simulator as well, exposing the electronics to high forces. For all situations were no 1 10/ 220 V power supply is available, nVis offers a battery powered control unit while the Z800 can be powered through a USB connection. The xSight, however, is connected through a small belt pack. The belt pack has to be within 1.3 m range to the HMD, but cables of 2 m to 100 m in length are available to connect belt pack and control unit.

[2] **Liquid Crystal on Silicon** is a micro-display technology mainly used in projection televisions. It uses liquid crystals on the surface of a silicon chip coated with an aluminized layer. A light source illuminates the chip and the reflection is displayed.

| Model | xSight 6123 | SX111 | SX60 | Z800 |
|---|---|---|---|---|
| Manufacturer | Sensics Inc. | nVis Inc. | nVis Inc. | eMagin Corp. |
| FoV Category | 3 | 3 | 2 | 1 |
| Horizontal FoV | 118° | 102° | 44° | 32° |
| Vertical FoV | 45° | 64° | 35° | 24° |
| Diagonal FoV | 123° | 111° | 60° | 40° |
| Resolution per Eye | 1920 × 1200 px<br>60 Hz<br>20 px/degree | 1280 × 1024 px<br>60 Hz<br>16 px/degree | 1280 × 1024 px<br>60 Hz<br>27 px/degree | 800 × 600 px<br>30 Hz<br>25 px/degree |
| Binocular Overlap | 63 % | 66 % | 100 % | 100 % |
| Weight | 400 g | 1300 g | 1000 g | 230 g |
| Display Technology | OLED | LCoS | LCoS | OLED |
| Color | 24 bit | 24 bit | 24 bit | 24 bit |
| Brightness | 394 cd/m$^2$ | 17 cd/m$^2$ | 102 cd/m$^2$ | 51 cd/m$^2$ |
| Contrast | 800:1 | 100:1 | 100:1 | 200:1 |
| Costs | not listed | $24,950 | $12,950 | $1,295 |

**Table 1.1:** Technical specifications of four different HMDs in comparison. All data was taken from the manufactures' websites and rounded to the next worse integral number if necessary. The HMDs are shown in Figure 1.5

**Figure 1.5:** Design of four different HMDs in comparison. In the top row: (a) Sensics xSight 6123, (b) nVis SX111. In the lower row: (c) nVis SX60, (d) eMagin Z800. Technical specifications are listed in Table 1.1. Pictures taken from [NVIS Inc., 2010; eMagin Corporation, 2010].

## 1.3 Overview of Motion Simulators

The development of motion simulators was driven by the need of the aerospace community to train pilots in safe environments. The American Air Force was the first to use mechanical motion simulators during the first world war. In a freely swinging seat, pilots were instructed on how to aim with the on board machine gun while the plane was tilting.

Organ constructor Edwin Albert Link Jr. invented the first pneumatic driven motion simulator and started selling his "combination training device for student aviators and entertainment apparatus" in 1929. A patent was issued in 1931 which describes the simulator in more detail [Link Jr., 1931]. The simulator soon rose attention of the United States Army Air Corps and during the second world war he sold more than 10,000 units [L-3 Communications Link Simulation & Training, 2010]. This first motion simulator was able to roll and pitch 3° on a universal joint. All instruments were simulated, but no vision system was featured at that time (Figure 1.6). Later models had three rotational DoFs with a range up to 10°.

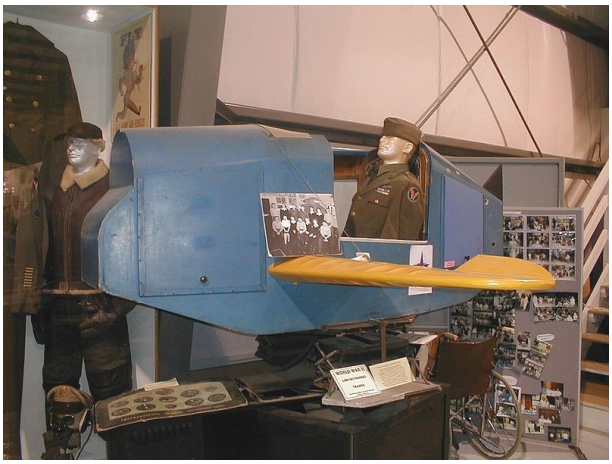

**Figure 1.6:** Link flight simulator at Warhawk Air Museum in Nampa, Idaho, USA

In 1948, Pan American was the first airline to own a civil Boeing B-377 Stratocruiser flight simulator. However, this simulator was stationary even through it featured a fully functioning cockpit.

First visual systems used a scaled mock-up landscape. A robotic arm moved a camera synchronously with the simulator according to the pilots control input while the camera images were displayed to the pilot.

### 1.3.1 Types of Motion Simulators

Over the years different ways to simulate motion evolved. The following subsection will provide an overview of the technology commonly used. However, todays largest simulators often combine several technological solution (Subsection 1.3.3).

### Hexapods

Octahedral hexapods are the most common technological solution for motion simulators. Six hydraulic struts move a platform with six DoFs in a limited workspace. They are commonly known as Stewart-Platforms although Stewart was neither the first to present a platform with six DoFs, nor had his invention much in common with recent octahedral hexapods. For simplicity we will rely on the more general term hexapod when meaning a octahedral hexapod.

The first hexapod with six hydraulic struts in a octahedral pattern was constructed by Gough and went into operation in 1954 as a tire testing machine (Figure 1.7a). His work was not published until 1962 [Gough and Whitehall, 1962]. Although hydraulic platforms with six DoFs existed before, he was the first one to use six struts all underneath the platform. Three years later, Steward presented a platform that was designed as a flight simulator (Figure 1.7b). His structure had three struts and each one was changing the angle of another strut. These other struts were finally acting on the platform [Stewart, 1965]. This arrangement had the disadvantage that the struts could not be moved independently from each other. Therefore, inaccurate control of the struts resulted in high mechanical stress on the joints holding the platform.

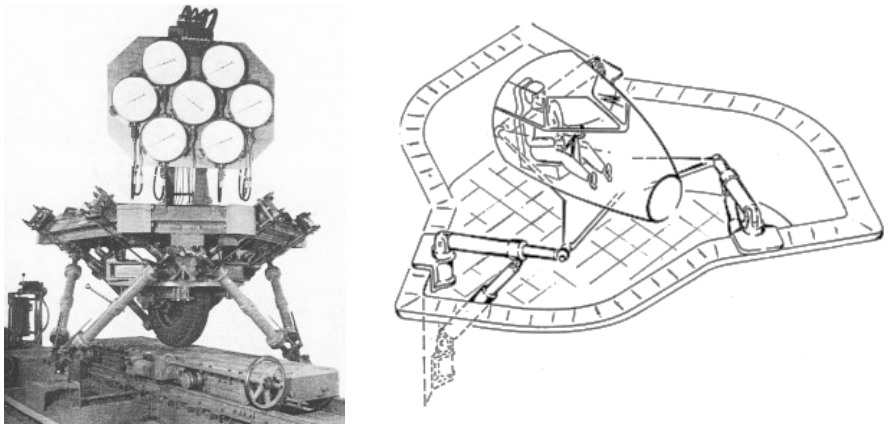

**Figure 1.7:** (a) First octahedral hexapod. The structure was intended as a tire testing machine. Picture taken from [Gough and Whitehall, 1962]. (b) The motion platform supposed by Stewart, the 'real' Stewart-Platform. Picture taken from [Stewart, 1965].

The first motion simulator based on a octahedral hexapod was patented in 1967 by Klaus L. Cappel [Cappel, 1967]. He was unaware of Gough's work and Stweward's paper was not published at the time he handed in his patent in 1964. His invention used six hydraulic struts in an octahedral pattern. This design was an improvement of Gough's layout since he added universal joints at both ends of the struts for the connection to the platform and to the foundation. In this way, the mechanical stress at the joints was reduced and the struts could be moved with less restrictions (Figure 1.8a). However, flexibility of hexapods is very limited when operated close to the workspace boundaries.

Nowadays all major airlines operate flight simulators which make use of this almost unchanged octahedral hexapod system (Chapter 1.3.3). NASA developed a low impact docking system based on the flexibility of a hexapod and installed it on the Hubble Space Telescope [Lewis et al., 2002].

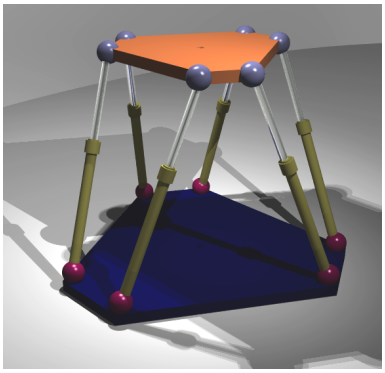


**Figure 1.8:** (a) Model of an octahedral hexapod. Blue and magenta balls represent universal joints. Published under GFDL. (b) Large Amplitude Multi-mode Aerospace Research Simulator (LAMARS) from 1975 operated by the United States Air Force. Picture taken from the US Air Force.

### Robotic Arms

Robotic arms are flexible, more precise and have a larger motion range compared to hexapods. Therefore, they are a well suited base for motion simulators. However, for a long time no robots that could move heavy loads fast and precisely were available. In 1975, the United States Air Force constructed a unique simulator based on a robotic arm. A cabin was attached through a wrist with three rotational DoFs to a long arm. Furthermore, the arm could be rotated vertically and horizontally adding up to five DoFs in total (Figure 1.8b).

In 2003, the robot manufacturer KUKA started selling a modified industrial robot with six joints as a theme park attraction. Several research organizations, like MPI and DLR, equipped this robot with visual feedback devices and use it as a full motion simulator (Chapter 2).

### Human Centrifuges

Human centrifuges were build to simulate sustained high accelerations. Thus, they were first used by space agencies with the aim to test the influence of accelerations higher than 1 g on the human organism when exposed for a long time. Indeed, air forces needed to train their pilots to safely fly maneuvers with sharp turns even at very high speed associated with high centrifugal forces.

Centrifuges constitute at least of a robotic arm with a cabin mounted on one end and a counterweight or another cabin at the opposite end. The structure spins around its center to create centrifugal forces oriented away from the center. Most seats are additionally mounted inside a gimbaled cabin which allows to vary the orientation of the centrifugal force relative to the human body during operation (Figure 1.9).

The most powerful centrifuge in operation today, the TsF-18 at the Yuri Gagarin Cosmonauts Training Center in Russia, is able to generate forces of up to 30 g (5 g are potentially deadly for an unprotected, untrained person). Each of the three interchangeable gimbaled cabins can be evacuated and air-conditioned to simulate high altitudes.

**Figure 1.9:** Human Centrifuge from 2006, build in Germany by AMST Systemtechnik GmbH. Picture taken from [AMST Systemtechnik GmbH, 2010].

#### Linear Robots

Motion simulators based on nothing but a linear robot are rarely used since they are incapable of simulating rotational motions. In applications where only one or two translational DoFs are needed, a seat on a linear moving sledge might become an economic option [Sövényi and Gillespie, 2007].

Car manufacturer including Renault and Toyota use a two dimensional linear robot system to hold a hexapod platform which simulates the rotations (Chapter 1.3.3). The NASA operates a motion simulator that combines a three dimensional linear robot with a tilting universal joint similar to the design used for Link's first simulators (Chapter 1.3.3).

### 1.3.2 Motion Cueing

In most cases it is impossible to simulate motion directly by mapping motion in all six DoFs in space onto six corresponding simulator axes. The workspace of all motion simulators is restricted and additional technical limitations are usually present depending on the chosen design. Thus, the desired motion must be properly scaled and adapted to fit into the motion bounds defined by the particular simulator. The references provide information on motion cueing algorithms as well as on a solution for our CyberMotion simulator [Nahon and Reid, 1990; Grant and Reid, 1997; Robuffo Giordano et al., 2010].

### 1.3.3 A Selection of existing Motion Simulators

In this subsection, we will introduce a selection of four powerful motions simulators. These simulators are still in operation today and serve for different applications. The combination of different simulator technologies as described above made these systems very powerful.

#### Desdemona

In 2007, TNO Human Factors together with AMST Systemtechnik GmbH finished construction of the Desdemona motion simulator. The main idea during the design phase was to combine

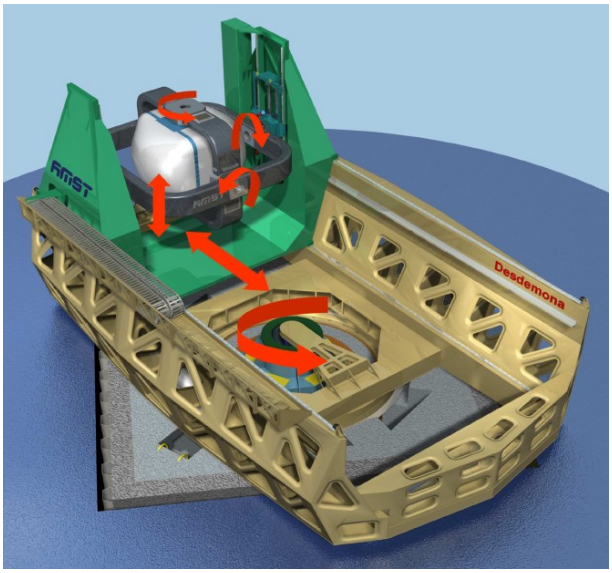


**Figure 1.10:** Desdemona motion simulator at TNO Human Factors in the Netherlands. The six DoFs are highlighted. Picture taken from [Roza et al., 2007].

the flexibility of a hexapod with the ability of human centrifuges to simulate sustained high accelerations. The final layout features a cabin in a fully gimbaled system without angular limitations which allows the cabin rotate continuously around any axis in space. The gimbaled system was mounted in a 2 m heave system that moves the cabin vertically which itself is located on a 8 m sledge that moves horizontally. The entire structure rotates continuously around the central axis of the sledge (Figure 1.10). With the heave system in the outer most position 4 m off the rotational axis, continuous accelerations of 3 g can be reached [Roza et al., 2007].

### Vertical Motion Simulator (VMS)

The NASA operates its VMS to explore, define and solve issues in both aircraft and spacecraft design [National Aeronautics and Space Administration (NASA), 2010]. The simulator has an interchangeable cabin which enables the NASA to perform research on different kinds of vehicles such as planes and spaceships (Figure 1.11a). In order to meet the special needs of these applications, the simulator was built in a tower. Its linear robot system allows movements of up to 18.3 m vertically and 12.2 m horizontally. However, forward/backward motion is limited to 2.4 m (Figure 1.11b and c). The cab is attached to the robot via a universal joint and a powered turntable. The turntable is used to simulate heading rotations while hydraulic struts roll and pitch the cabin at the joint. In total the system has six DoFs.

### Lufthansa Flight Training Simulators

German regulations require pilots to frequently train extreme flight situations in simulators. Lufthansa Flight Training GmbH, a division of Lufthansa AG, operates more than 40 flight simulators for pilot training in mainly Frankfurt and Berlin. All theses simulators hold real cockpits and each simulates only one very special aircraft configuration. Up to 200

**Figure 1.11:** NASA's Virtual Motion Simulator (VMS). (a) Interchangeable cabin on the motion base. (b) The motion base seen from the top of the tower in the lowest and (c) the highest position at 18.3 m. Pictures taken from [National Aeronautics and Space Administration (NASA), 2010].

speakers simulate real acoustics of a plane and most recent simulators are equipped with a 200° by 40° FoV projection system. Most simulators are based on a large hexapod platform (Figure 1.12). Lufhansa Flight Training offers data sheets of all their simulators on `http://www.lufthansa-flight-training.de`.

### Toyota Driving Simulator

Toyota operates one of the most complex motion simulators. It is mainly used for safety research and is able to simulate complete car systems including distance sensors and other parts of the car electronics. Toyota claims that the simulator will be used to develop "active safety technologies with the aim to produce cars that prevent accidents" [Toyota Motor Corporation, 2010].

The central dome of 4.5 m in diameter holds an exchangeable full size car mock-up. The car is mounted on a vibration simulator which has a vertical gain of 5 cm. This system is located on a turntable which allows turns of 330° in both directions. The dome forms the upper part of a hexapod platform which is mounted on a 35 m × 25 m linear robot system itself (Figure 1.13). The hexapod is able to produce tilts with a maximum angle of 25°. All together, the simulator has ten DoFs. Eight projectors are used to create a seamless 360° projection on the curved inside wall of the dome.


**Figure 1.12:** Lufthansa's A380 motion simulator at Frankfurt Airport. A mass of 15 t is moved through a hexapod platform. Picture taken from `www.lufthansa.de`.

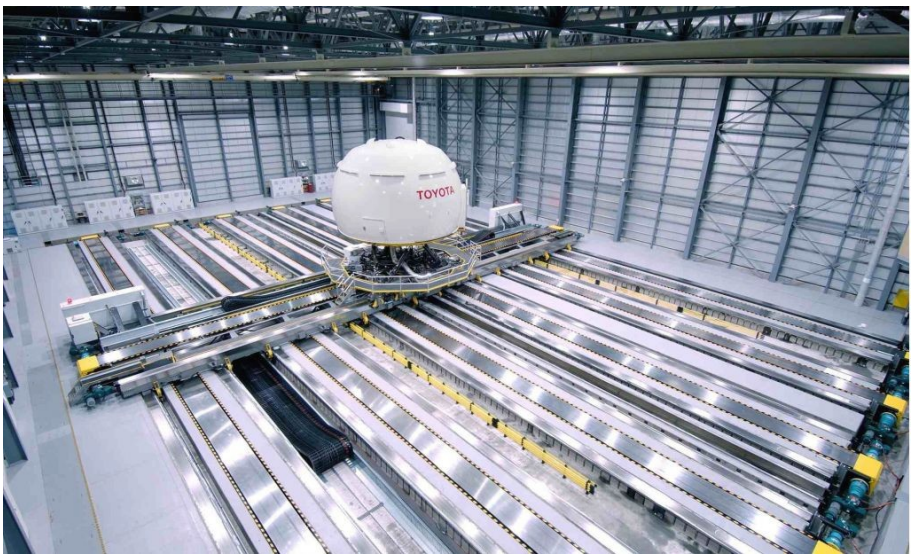


**Figure 1.13:** Toyota's driving simulator. The dome with a mock-up car inside is mounted on a hexapod which itself is located on a two dimensional cartesian platform. Picture taken from [Toyota Motor Corporation, 2010].

# Chapter 2

# CyberMotion Simulator

The CyberMotion simulator is a motion simulator based on a robotic arm. It was derived from KUKA's Robocoaster which was designed as a thrill ride and is located, among other amusement parks, in several "Legoland" theme parks. The Robocoaster itself is a modified version of KUKA's heavy duty industrial robot KR500 which is mainly used in automotive industry (Figure 2.1) [Kuka AG, 2010].

This chapter will provide a technical description of the simulator, introduce the most important equipment, and explain how the simulator is interfaced through the control PCs.

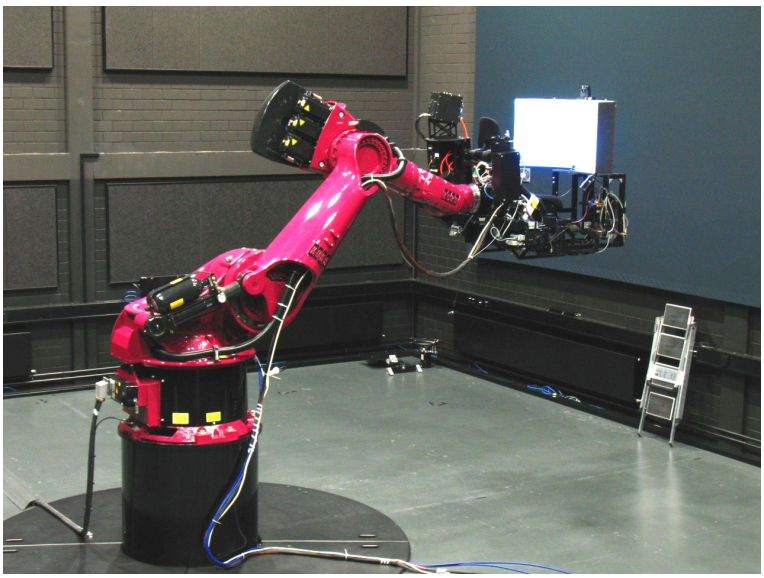

**Figure 2.1:** RoboLab with CyberMotion simulator and mounted projection screen in central position.

## 2.1 Technical Description

Being the only robot that meets the strict requirements for moving humans [Kuka AG, 2010], the MPI for Biological Cybernetics acquired a Robocoaster in 2005. It was the first Robocaster

| | |
|---|---|
| Robot type | KR 500 TÜV |
| Number of axes | 6 |
| Accuracy | $\pm$ 0.15 mm |
| Length of the arm | 2826 mm |
| Engine system | electro mechanic servo motors |
| Max. supplementary load for equipment | 100 kg |
| Total weight | 2350 kg |
| Covered work space | 68 $m^3$ |
| Size of the RoboLab | 12 m x 12 m x 12 m |
| Noise level | $<$ 75 dB(A) |
| Weight and size constraints for passengers | max. 100 kg, 140 cm – 195 cm |

**Table 2.1:** Specifications of the CyberMotion simulator

| **Axis** | **Motion bounds** | **Velocity limit** | **Acceleration limit** |
|---|---|---|---|
| 1 | $-120°$ to $+120°$ | $60°s^{-1}$ | $160°s^{-2}$ |
| 2 | $-127°$ to $-42°$ | $48°s^{-1}$ | $160°s^{-2}$ |
| 3 | $-29°$ to $+77°$ | $48°s^{-1}$ | $160°s^{-2}$ |
| 4 | $-180°$ to $+180°$ | $48°s^{-1}$ | $40°s^{-2}$ |
| 5 | $-45°$ to $+45°$ | $95°s^{-1}$ | $199°s^{-2}$ |
| 6 | $-180°$ to $+180°$ | $119°s^{-1}$ | $199°s^{-2}$ |

**Table 2.2:** Limitations of the six revolute joints of CyberMotion simulator. The listed motion bounds and velocity limits can be used without any constraints. They are followed by an additional emergency stop range until low level software bounds are reached. Maximum accelerations can be reached for short times only to prevent the engines from overheating.

to be modified and used as a motion simulator in scientific research. General specifications of the CyberMotion simulator are outlined in Table 2.1.

The base of the simulator was mounted onto a foundation in the center of our RoboLab, a cubic hall of 12 m in all dimensions. The robotic arm has six electronically powered revolute joints in a configuration similar to a human arm. This anthropomorphic layout allows the robot to position the end-effector within the workspace by only using the first three axes. Orientation is controlled with the help of axis 4 to 6 which function similar to a human wrist (Figure 2.2).

The robotic arm of the CyberMotion simulator with six DoFs bypasses the limitations of simulators based on hexapod platforms with six hydraulic struts (compare Chapter 1.3.1). Therefore it is possible to perform motions in a very large range and less motion cueing is required to fit desired motions into the workspace of the simulator. The configuration of all joints as well as axis limitations ensure that the seat at the end effector of the robotic arm is physically incapable of touching itself or the surrounding walls. Work space restrictions as well as limitations in the angular velocity and acceleration are listed in Table 2.2.

Violations of the limits are monitored by an internal robot model. A controller reads the

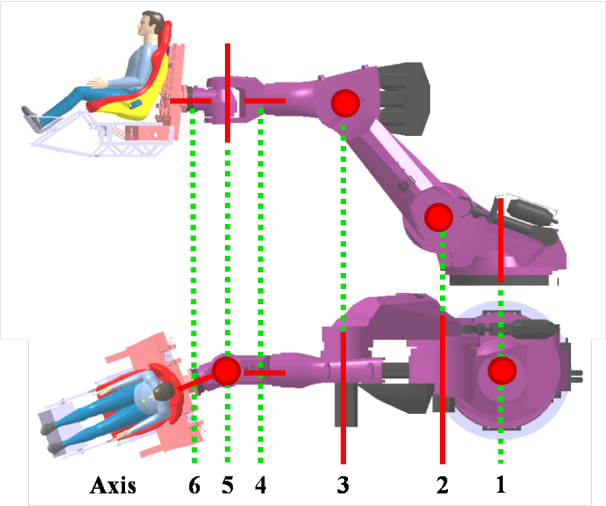


**Figure 2.2:** Location and orientation of the six revolute joints of the CyberMotion simulator. (a) The upper graph shows the simulator in a side view while (b) the lower one is a view from the top.

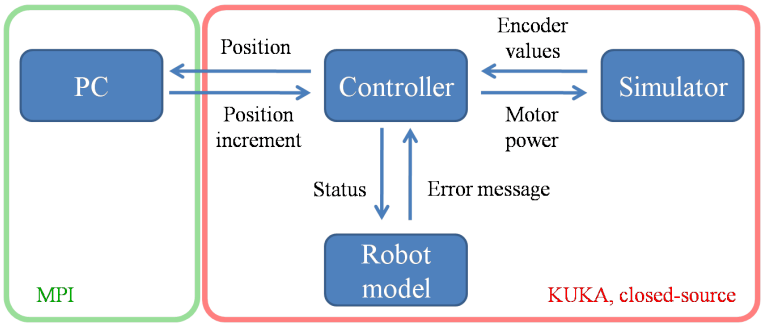


**Figure 2.3:** Interaction graph between control PC, controller, robot model and simulator. Controller and robot model form one physical unit.

status of the encoders on all axes, communicates with the model to check for violations, regulates the power to the motors, and maintains a network interface with the external world. Both controller and model, developed by KUKA as a proprietary software component, cannot be accessed or bypassed by normal users. Position information of the robot is sent once every 12 ms via UDP connection to an interfacing PC that provides position increments within the next 12 ms. If this handshake fails, the increment is set to zero, thus possibly violating an acceleration limit due to a sudden stop of the moving simulator. The interaction between PC, controller, model and simulator is shown in Figure 2.3.

A detailed technical description can be found in [Teufel et al., 2007].

## 2.2 Force Feedback Steering Wheel

A force feedback control device is known to increase the control accuracy in applications where a high level of precision is required. This was shown for dynamic control tasks in general [Forsyth and MacLean, 2006] and precise surgeries as well as control of land vehicle in particular [Wagner

et al., 2007; Steele and Gillespie, 1994].

In order to provide an advanced force feedback interface, the CyberMotion simulator can be equipped with the 'SENSO-Wheel SD-LC' force feedback steering wheel from Sensodrive GmbH (Figure 2.4) [Sensodrive GmbH, 2010].

A powerful motor is connected to the wheel without any transmission to increase angular resolution. The internal controller of the wheel has a cycle time of 1 ms and is therefore able to adjust the force at a rate of 1000 Hz. The motor is able to simulate adjustable hardware end stops of the continuously tuning wheel. Technical data of the wheel is provided in Table 2.3.

Wheel and controller are mounted in front of the seat on the simulator. For safety reasons, the power supply is located off the robot and cables along the arm deliver the operating power of 48 V to the controller. The wheel is interfaced using bidirectional CAN-bus communication.

The controller implements a state machine with four states (Figure 2.5). Force is only active in 'On'-state, but the wheel position can be read in any state. In order to keep the communication on the bus low, active request is necessary to read the orientation of the wheel. At least one request has to reach the controller every 50 ms, otherwise the state machine switches into the 'Error' state and thus disables the force for safety reasons. All general parameters, such as end stops and force levels, are set using stepwise transition requests towards the 'On' state. Varying forces may be set through position requests with a frequency of up to 1000 Hz. Optionally, a parametrized spring damper model is provided for simplification.

## 2.3 Head Tracking System 'Track IR 5'

An inconsistency of visual and vestibular perception is known to cause motion sickness (Subsection 1.1.3). Thus, head tracking might be an important issue even in applications without desired head movements. On a motion simulator, due to high accelerations, unintentional head motion of small magnitude in a high frequency domain occurs. It is believed that head tracking improves the users comfort on motion simulators when using HMDs. However, a scientific investigation of this interaction is still an open problem.

During this work, the CyberMotion simulator was not equipped with a head tracking system. To find a simple yet cheap solution, we acquired the head tracking system 'Track IR 5' from Naturalpoint [NaturalPoint Inc., 2010]. This low cost head tracking system was mainly designed for gamers and turned out to be highly accurate with the provided demonstrational program. A sample rate of 120 Hz assures a low latency of the small device (3.81 cm × 5.08 cm × 1.45 cm, Figure 2.6a).

The tracking system emits infrared light from four LEDs. A tracking clip on a base ball cap with three markers and known distance between them reflects the light back to an infrared sensitive camera (Figure 2.6b). The computer calculates position and orientation of the clip within the viewing frustum of the camera. Since only three markers are used to calculate the position in a six dimensional space, certain limitations apply. Only orientations up to a certain angle are reported.

For testing purposes, we carved foamed polystyrene to hold the camera and covered it with black tape. The camera was then mounted on top of the projection screen (Figure 2.7b). We attached the reflective clip on top of the Sensics HMD (Chapter 3) at the same position as it would have been on a base ball cap relative to the eyes (Figure 2.7a). The clip was always within

**Figure 2.4:** Force feedback steering wheel 'SENSO-Wheel SD-LC' from Sensodrive. Picture taken from [Sensodrive GmbH, 2010].

| | |
|---|---|
| Angular resolution | 0.009° |
| Torque resolution | 0.03 Nm |
| Rated torque | 7.5 Nm |
| Maximum torque | 16.5 Nm |
| Interface | CAN-bus (500 kBaud) |
| Cycle time | 1 ms |
| Power supply | 48 V, 13 A |
| Weight | 9.0 kg |

**Table 2.3:** Technical data of the force feedback steering wheel 'SENSO-Wheel SD-LC' used on the CyberMotion simulator.

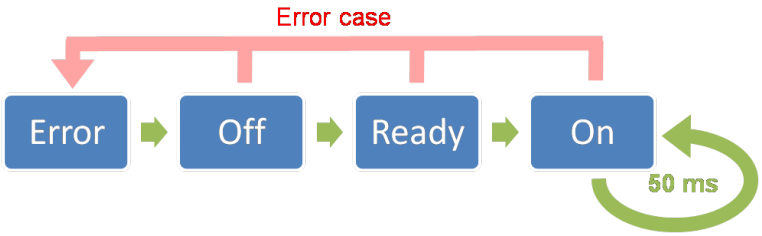


**Figure 2.5:** Graph of the state machine used in the steering wheel controller. In state 'On', force is activated an the controller has to receive a CAN message once every 50 ms. It switches into the 'Error'-state otherwise.

the FoV of the camera in all possible head positions.

In spring 2010, NaturalPoint offered two different APIs to interface the 'Track IR 5'. One supported the 'Track IR' only and was available for registered game developers exclusively. The other supported more sophisticated camera systems and was available for the general public free of charge.

Using the free API, we designed a class that provided tracking capability to the program controlling the simulator. At instantiation time, it sets up the communication to the camera and activates the infrared light sources as well as the camera. During runtime, it grabs frames from the camera and hands them to the calculation module to retrieve the coordinates of the head.

During first tests, we found that the orientation data suffered from a strong noise that was not observed in the demo application. However, this demonstration made use of the closed game developer API. It turned out, that the free API did not support our recent version 5 of the 'Track IR' but only version 4 with a higher lag and only a $10^{\text{th}}$ of the resolution. A low pass filter was implemented to reduce the noise with limited success. The noise was mainly in the same frequency domain as the head movements on the moving simulator.

Unfortunately, we finally had to drop the head tracking support. Since it was not possible to compensate the vision for undesired head movements, we had to add control conditions without physical motion to all experiments. A larger performance difference between physical motion and a stationary robot with the use of an HMD compared to a projection system would eventually lead to the assumption that head tracking is important on a moving simulator.

## 2.4 Operational Setup

The control software of the simulator was split in two parts. The main part ran on the 'Control PC' while the visualization was located independently on the 'Vision PC' for performance reasons. Both were connected in a local network together with the 'Controller'. The CAN-bus was used to interface input devices as the force feedback steering wheel and a flight control stick (Figure 2.8).

### 2.4.1 Network Communication

The network communication via UDP packets between the control PC and the vision PC relies on the free library XdevL [Terzibas, 2010]. A server was set up on the control PC that sends out position information once every controller clock cycle.

We designed the UDP packet to hold two independent sets of position and orientation data. This allows future developers to send coordinates for a second moving object. An integer for both a time stamp and a package number gives the ability to track packet history and recognize a potential packet loss if necessary. Additionally, a third integer field is provided for the transmission of additional data for the individual experiment.

The visualization software on the vision PC makes use of two classes to read the position data from the network. One class provides the interface for the rest of the visualization and encapsulates an independent thread that listens for new incoming UDP packages. The thread writes new data into thread save variables and grants save access from the observing class. This

**Figure 2.6:** Head tracking system 'Track IR 5' from Naturalpoint. (a) The 'Track IR 5'. An infrared camera with four powerful infrared LEDs at its side is located behind the black window. LEDs on the side indicate the status of the system. (b) Reflective clip attached to a base ball cap. The system tracks the three reflective markers and calculates orientation and position from their relative position to each other. Pictures taken from [NaturalPoint Inc., 2010]

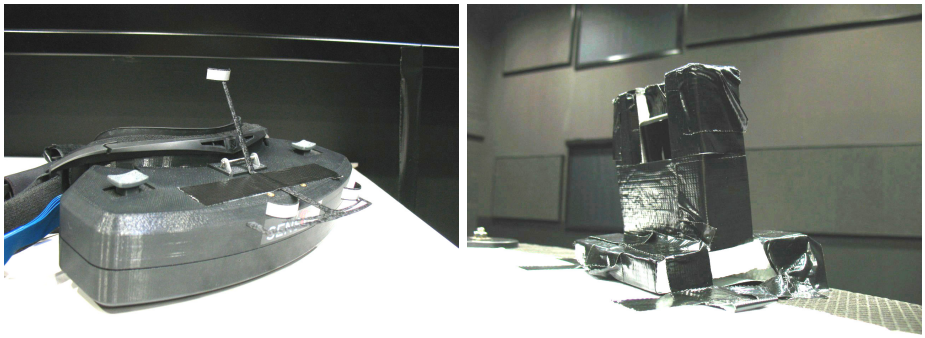

**Figure 2.7:** (a) Sensics HMD with attached reflective clip on top. (b) 'Track IR 5' in mounting made from foamed polystyrene on top of the projection screen on the CyberMotion simulator.

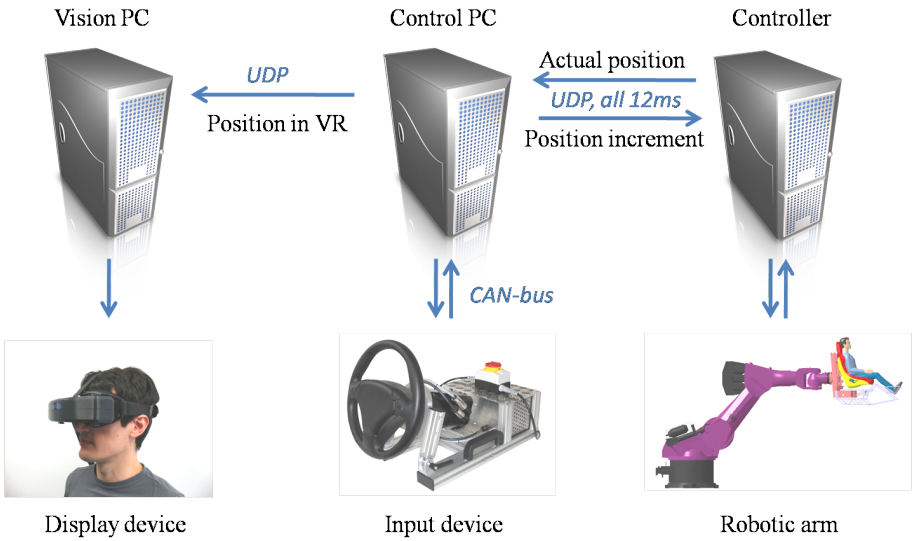


**Figure 2.8:** Interaction graph between the different subsystems which together form the CyberMotion simulator.

way, the outer class always returns the most recent position data from the control PC. All other parts of the visualization are covered in Section 3.4.

### 2.4.2 Control Software

The development of the software on the control PC started off from existing code for an helicopter hovering experiment. However, the lack of a solid object oriented design resulted in very inflexible program code over the years. Whenever a new experiment was designed, old code was adapted and changes became necessary in almost all parts of the program. Thus, we decided to rewrite large sections of the code.

In Figure 2.9, we outlined the most important program components and their interaction. The elements on the left correspond to rewritten object oriented classes and interfaces, and those on the right side of the dotted line to old unchanged parts of the program.

The program is triggered through the clock signal of the controller which sends out position information once every 12 ms. The control program sends position increments back to the controller after a limit violation check within the following clock cycle of 12 ms.

We decided to keep the state machine, the communication interface with the simulator and the violation control in the current state for safety reasons. This part and especially the violation control was extensively tested in many possible circumstances by our technicians. The state machine keeps track of the current simulation state (Figure 2.10). The cycle starts with a stationary simulator in the condition selection state. While the program waits for a user input, it sends increments of 0 to the simulator. Following the selection of a condition through the experimenter, control is delegated to an abstract vehicle model in the experiment state. At the end of an experimental run, the vehicle model hands back control and requests a soft break followed by a reset of the robot back into the starting position. Both processes were implemented as linear ramps over time in the velocity (respectively position) domain. The simulation may be stopped at any time which causes the program to directly move to the break state and terminate afterwards.

While restructuring the code, competence was shifted towards the vehicle model and the tracking of input devices was removed from the old core around the state machine. Furthermore, we extended the condition selection and added the possibility to use an automated selection. This allows to run experiments with different conditions in a predefined pattern which helps the experimenter to avoid mistakes during the conduction of an experiment.

In order to keep the program flexible, we designed the most commonly changed classes as abstract classes. For every new experiment, only a new vehicle model implementing the abstract vehicle model class has to be be written and plugged into the existing structure. Additionally, it is now possible to switch vehicle models and input devices even at runtime. Input devices became interchangeable very easily upon availability and the integration of new input devices was simplified.

When control is delegated to the vehicle model, it can rely on additional data stored in a parameter file. This gives the possibility to add disturbing noise to the model or to change parameters over time in a predefined way. The file reader allows to read any number of lines with a flexible number of columns from a simple text file. Data is accessible through line and column number. After the calculation of a new position, it is sent to the vision PC as described earlier. The corresponding position increment is sent to the simulator.

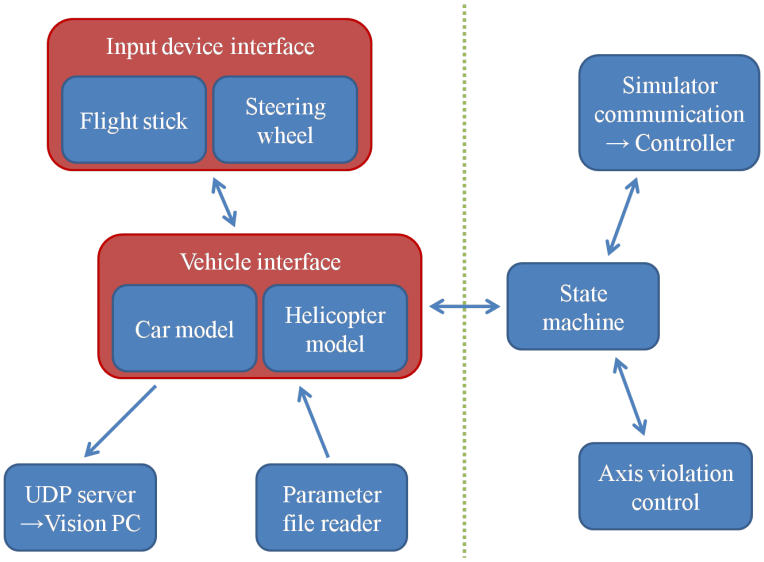


**Figure 2.9:** Design chart of the control software running on 'Control PC'. The part left of the dotted line was rewritten and improved in object oriented C++. The right part including the well tested axes violations control was left untouched for safety reasons.

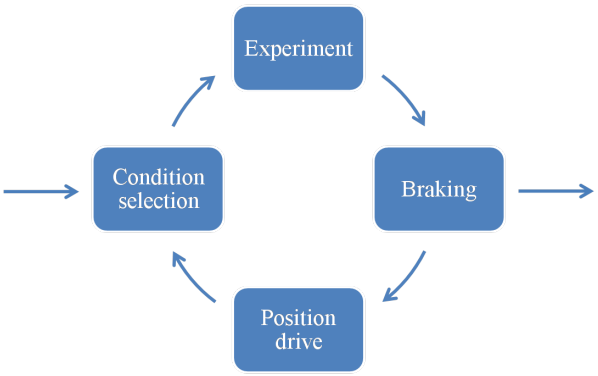


**Figure 2.10:** State machine of the simulation control algorithm. In the initial 'Condition selection' state, the program is waiting for a program selection. While in the 'Experiment' state, control is handed to the vehicle model. After an experiment run, the simulator stops in the 'Braking' state. When in the 'Position drive' state, the simulator moves back to the starting position for the next run. The program can be left through the 'Breaking' state only to ensure a stationary simulator at the termination of the program.

## 2.5 Safety Aspects

Safety aspects were the main criteria during the whole software development process. All new and improved programs were tested on a simulated robot system first. We equipped our software with smooth emergency braking procedures that are able to take over control immediately at any time. The software prevents any violation of limits that would cause sudden emergency brakes with high accelerations activated by low level controls.

Two operators trained in emergency rescue procedures have to be present during operation of the simulator. Magnetic switches ensure that the seat belt remains fastened and nobody enters the work space while the robot is in motion. Sick and especially large or heavy people are excluded from the ride. Everybody has to sign a consensus before entering the simulator.

# Chapter 3

# Head Mounted Display 'Sensics xSight 6123'

HMDs from Sensics feature one of the widest horizontal FoV that is commercially available at the moment. Most other systems with a wider FoV were either discontinued or made as a custom solution for single customers. For virtual reality applications at the MPI for Biological Cybernetics, the Sensics xSight 6123 with a FoV of 118° horizontally and 45° vertically was acquired in 2009 (Figure 3.1). Since a cable long enough for the use in our tracking lab was not available yet, we decided to integrate it into the CyberMotion simulator first.

In the following sections, we will provide a technical description of the HMD and explain the integration into to simulator on both the hardware and the software side.

**Figure 3.1:** Sensics xSight 6123 HMD. The HMD is mounted on the head with three adjustable strips that meet at the back of the head were a nob can be used to adjust the tension.

## 3.1 Technical Description

For the xSight 6123, Sensics patented a unique technology to stitch six micro displays to one continuous image for each eye. This allows the usage of small OLED displays with a low

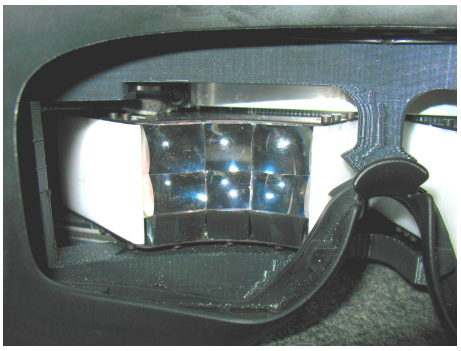

**Figure 3.2:** Left eye piece of our xSight 6123 HMD holding six micro displays and its lenses.

resolution to form a large image with high resolution without the need to use heavy LCoS technology. Thus, the xSight 6123 presents an image of $1920 \times 1200$ pixels in front of each eye across a FoV of 118° horizontally and 45° in total while the weight does not exceed 400 g [Sensics Inc., 2010].

Each display is equipped with a special ground lens that spreads the light. One end of the lens is flat and rests on the display while the other is framed in a matrix together with the lenses from the neighboring displays (Figure 3.2). The transition between the lenses becomes invisible since the eye is unable to focus on a structure that close to the eye. Sensics offers to upgrade the system and add additional rows of displays and lenses at a later time.

All six displays were made by eMagin and feature a resolution of $800 \times 600$ pixels each. eMagin uses the same displays for its consumer market HMD Z800. Displays and lenses are mounted in an eye piece that is rotated outwards by 16.75° and can be moved sidewise to fit the user's eye distance. A casing holds the eye pieces and is shielded against the outside world with the help of a ski goggle rim. An external control unit is used to power the displays.

The control unit splits the $1920 \times 1200$ pixel input signal into six $800 \times 600$ pixel images for the individual micro displays in each eye. Simple logic in programmable FPGAs[1] is used to ensure a fast mapping of one pixel from the input to each pixel on the output.

A configuration file is used to specify the position of each display in polar coordinates on a hemisphere around the retina of each eye. Sensics provides a tool that reads this file, calculates the resulting pixel mapping between input signal and the six displays, and rewrites the FPGA configuration via a USB connection. However, no tool was provided to generate the specification file yet. Therefore, we were forced to find a good configuration manually. Furthermore, the rectangular and plane displays are treated as if they would cover a portion of the hemisphere surrounding the eye. No possibility is provided yet to remove pincushion distortions[2] and keystone effects[3] caused by the projection of the flat images onto the round hemisphere. Consequently,

[1] A **Field-Programmable Gate Array** is an integrated circuit designed to be configured by the customer or designer after manufacturing. FPGAs contain programmable logic components called "logic blocks", memory elements, and a hierarchy of reconfigurable interconnects between the blocks. Logic blocks can be configured to perform complex combinational functions, or merely simple logic gates like AND and XOR. Adapted from `http://en.wikipedia.org/wiki/Field-programmable_gate_array`.

[2] **Pincushion distortion** describes the optical effect of lines that are bowed inwards, towards the center of an image, like a pincushion. Image magnification increases with the distance from the optical axis.

[3] The **keystone effect** is caused by the attempt to project an image onto a surface at an angle. It is a distortion of the image resulting in trapezoid dimensions, the shape of an architectural keystone.

it is impossible to find a perfect transition between two neighboring displays. Thus, we tried to maximize the quality of the overlap in the central optical region and accepted a loss of quality towards the periphery.

At the moment, only a direct mapping of exactly one pixel from the input to each pixel on the output is supported. In some areas of the image, pixels from the input might occur twice or even more often in the output while others are not displayed at all. Unfortunately, no anti-aliasing technique to map more than one input pixel weighted to the output was implemented in the control unit to solve this issue.

In OLED displays, the intensity of each color fades at a different rate over time. Blue sub-pixels fade faster than red or green ones. Thus it is important to recalibrate the color settings regularly. We used a tool provided by Sensics to calibrate the colors on white, red, green and blue backgrounds of different gains. The control unit was added to the local network for this procedure and interfaced through a TCP/IP connection.

## 3.2 Setup on the Simulator

Both, HMD and control unit are mounted on the simulator. They are connected through a belt pack that holds the display drivers. The control unit is located in a metal frame on the side of the first axis. At that location, only low accelerations act on the circuit boards. Since the belt back has to be within 1.3 m range to the HMD, it was mounted to a solid steel plate at the right shoulder of the user. A custom made trunk cable of 10 m in length was used to connect belt pack and control unit along the robotic arm (Figure 3.3).

The control unit receives a double DVI input signal of $1920 \times 1200$ pixels from our vision PC. Both are connected through two 30 m shielded copper cables. The control unit does not send out an EDID signal that is used by the graphics hardware to detect the connection of a display device. Therefore, the use of a 'Gefen DVI Detective' to emulate a connected device became necessary to ensure a reliable image generation for both eyes. The channel for the left eye was split and additionally displayed on a monitor inside the control room for supervision (Figure 3.4).

## 3.3 3D Engine OGRE

We decided to use the free open source 3D engine OGRE from Torus Knot Software for our experiments [Torus Knot Software Ltd., 2010]. OGRE is an acronym for "Object-Oriented Graphics Rendering Engine". It was written in C++ and is designed for high cross-platform performance. Both, DirectX and OpenGL are supported on the hardware side.

OGRE holds all elements of the virtual world in a hierarchal scene tree of scene nodes. All objects and cameras are attached to a node and transformations are applied to the nodes only. Several rendering strategies are available to process the scene graph, depending on the need of the particular environment. A well documented plug-in interface allows the community to contribute to the project. Thus, it is possible to design complex environments even without a detailed knowledge in 3D rendering technologies.

Our work made use of the plug-in "PagedGeometry Engine" originally by John Judnich to build up a forest environment. A black and white hight map is processed to generate the shape

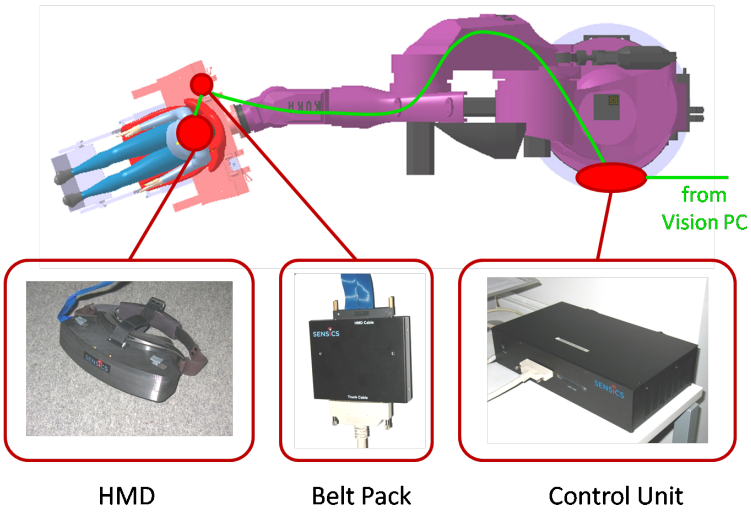


**Figure 3.3:** Integration of the xSight 6123 HMD into the CyberMotion simulator. The control unit was mounted on the first axis of the simulator while the belt pack is located next to the HMD at the seat. The signal is transmitted from the control unit to the belt pack via a special 10 m trunk cable. The HMD is connected directly to the belt pack.

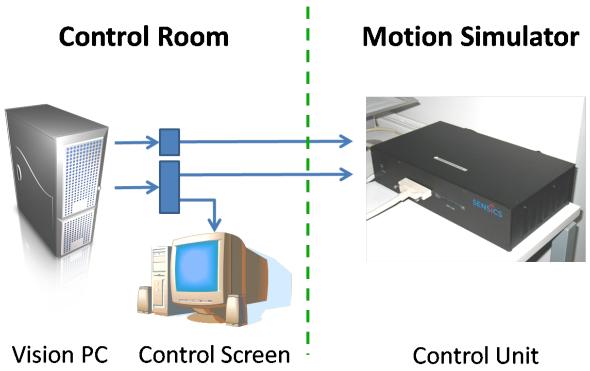


**Figure 3.4:** Configuration of the image generation for the xSight control unit. The signal for the left eye is transmitted to the control unit and a screen for supervision through a DVI switch while the right channel is connected via a 'Gefen DVI Detective'. Two 30 m DVI cables were used to span the distance between the control room and the simulator.

of the terrain. Since the size of our landscape combined with the wide FoV of the HMD reached the computational limits of our vision PC, we decided to use a uniform gray sky instead of a texturized sky box. Gray fog was used to fade out objects in a distance of 1500 m.

A detailed documentation can be found on the project's website `http://www.ogre3d.org`.

## 3.4 Integration of the HMD

To interface the xSight HMD, we designed a new class 'advancedCamera' that implements all methods known from the original OGRE camera class. Our class holds three instantiations of the original OGRE camera class. While two are used to render the image for the left and right eye, the third can be used as an additional scene camera for demonstrations and the experimenter's control screen (Figure 3.5). Our class provides support for the xSight 6123 and Z800 HMDs as well as for the projection screen on our simulator. With an adaption of the parameters, the SX111 could be used as well. We decided not to inherit from OGRE's camera class in order to render only as many cameras as needed for each device and application. However, since we implemented all methods of the original camera class, the design of a new environment remains the same. For the integration of our class into an existing scene, only declaration and instantiation of the camera have to be adapted.

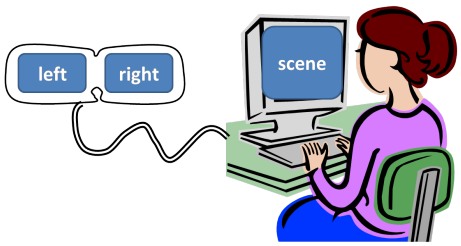


**Figure 3.5:** Purpose of the three cameras in our class 'advancedCamera'

For performance reasons, we decided to show the image for the left eye on the control screen. Thus, we saved the computation time for the additional third scene camera.

The correct setup of the two cameras powering the HMD in an OGRE environment turned out to be time consuming and difficult. Sensics provides configuration files for expensive major rapid prototyping 3D environment software such as 3DVIA Virtools and WorldViz, but no sufficient documentation of the camera parameters in general. Thus, reverse analysis of WorldViz configuration files together with measurements revealed the necessary information on how to set up the cameras for the HMD in OGRE. However, OGRE does not support Euler rotations. Instead, all rotations are carried out one after the other relative to the camera frame at the time of the rotation (Figure 3.6).

Therefore, a stepwise procedure was implemented to carry out all transformations in the right order (Figure 3.7). In between the rendering of two images, both cameras are at the same position facing into the same direction. First, roll and heading rotations are applied on all cameras. The heading rotation is always performed around the vertical axis of the world frame, thus both rotations are invariant and the order is not important in this step. The resulting x-axis of the camera (pointing to the right) in the world frame is stored for the later pitch rotation. Second, the cameras are translated relative to the new camera orientation. Since pitch rotations

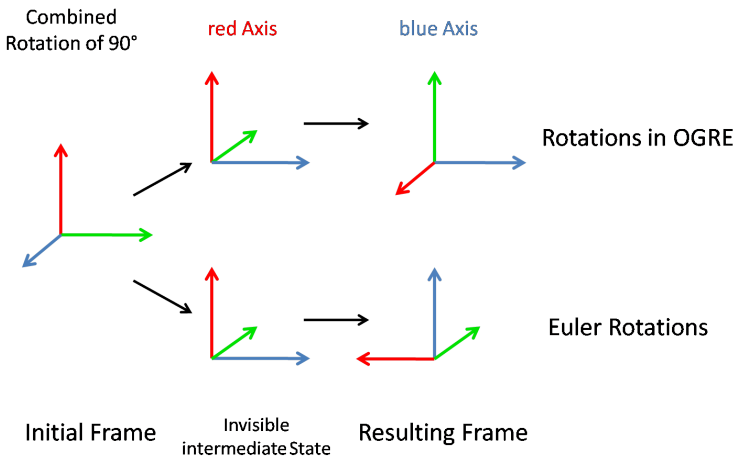


**Figure 3.6:** Euler rotations compared to rotations in OGRE. With Euler rotations, all rotations are defined with respect to the initial coordinate frame. OGRE, in contrast, processes all rotations individually one after the other each with the last frame as reference.

were not applied yet, the movement is ensured to be in the horizontal plane. Third, the two cameras for the HMD are separated by a predefined eye distance if stereo vision was enabled. In the next step, these cameras are rotated outwards 16.75° to meet the hardware design as described above. Finally, the pitch rotation around the previously stored axis is performed. After the image was rendered, the last three steps are revoked.

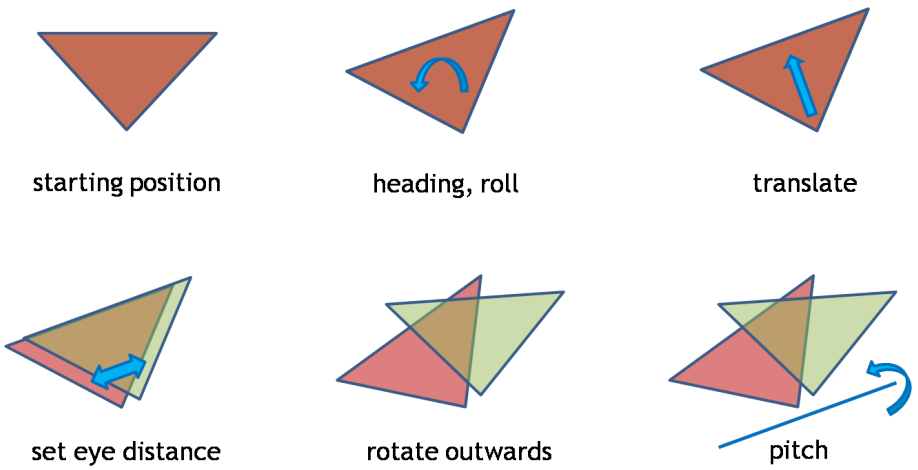


**Figure 3.7:** Camera transformations that are applied to display a stereo image inside the HMD. The camera for the left eye is outlined in green while the right one is shown in red. (a) Both cameras at the same position in the beginning; (b) cameras after heading and roll rotations were applied; (c) cameras after the translation step. (d) Cameras were separated by the predefined eye distance of 6.5 cm and (e) rotated outwards by 16.75° before (f) the pitch rotation using the frame from step (b) is applied.

# Chapter 4

# Experiments

After the integration of the xSight 6123 HMD into the virtual reality setup CyberMotion simulator, we tested the influence of the HMD compared to the projection system on the performance of a human operator on vehicle control tasks. Therefore, different experiments were designed.

First, we investigated the support of a wide FoV in flight control tasks with the projection system only. Since the limited workspace of simulators requires motion cueing and thus results in slightly inaccurate motion feedback, we compared different types of motion feedback. These experiments were designed as preliminary tests only. It turned out that a wide FoV does not improve a pilot's performance even under disturbed motion feedback.

Second, we investigated a slalom tasks in a driving simulation. We expected that a wide FoV is more important while navigating on the ground. The focus was shifted to the comparison of the HMD and the existing projection screen. We found that driving precision was highest with the projection system while neither motion nor a wide FoV improved drivers' performance.

The work on driving simulation was accepted for the Driving Simulation Conference 2010 in Paris, France [Grabe et al., 2010].

## 4.1 Tests on Flight Control Tasks

It is well known that large projection screens with wide FoV provide motion cues in the periphery of the visual field that can result in a greater sense of vection [Hettinger and Riccio, 1992; Mohler et al., 2005], more accurate navigation abilities [Alfano and Michel, 1990], and more accurate perception of self-motion [Pretto et al., 2009]. Constraints of the simulator require the use of motion cueing (Subsection 1.3.2). Thus, physically inaccurate motion might disturb the pilot when controlling a vehicle in a closed-loop motion simulation. Since visual input dominates vestibular information in a human [Ishida et al., 2008; Wright et al., 2005], we want to investigate whether a wider FoV improves the ability to control a flight vehicle even under disturbed motion conditions.

This experiment was designed as a preliminary test for the influence of different FoV sizes on flight control tasks with physically inaccurate motion feedback due to motion cueing. Since the Sensics xSight HMD was not available at the time of this experiment, no inter-device differences were examined. Thus, the aim of these experiments was to collect information for the design of a final experiment with both the projection screen and the HMD in comparison.

Two different experiments were conducted. In the first, subjects had to stabilize a hovering vehicle similar to a helicopter. In the second, a flight device with a constant speed had to be kept on a straight line of flight. These experiments were chosen because they reflect a range of experiments done on the CyberMotion simulator [Nieuwenhuizen et al., 2009; Robuffo Giordano et al., 2010]. Furthermore, we expect that these tasks require a good sense of vection and a wide FoV should help the pilot to perform well. Since it was shown that a hovering task requires a full motion feedback [Nieuwenhuizen et al., 2009], the influence of incorrect movements can be expected to be high in these tasks. Static conditions were added for control (Section 2.3). The design of the second experiment was influenced by Patterson et al. [Patterson et al., 2006] who chose a similar task to investigate the influence of the richness of an environment on flight control tasks.

### 4.1.1 Experimental Setup

#### Apparatus

We equipped the CyberMotion simulator (Chapter 2) with a two DoF flight control stick as commonly used in helicopters for this experiment. The virtual vehicle was controlled in closed loop. The projection system (Subsection 1.2.1) with a horizontal FoV of 90° and a vertical FoV of 45° was used to provide visual feedback.

#### Vehicle Simulation

In order to reduce the amount of training, we simulated a simplified helicopter model for the first series of tests. Control of the vehicle was restricted to the velocity of lateral motion. Lateral translations were mapped into planar circular trajectories with a radius of 3.1 m by rotating axis 1 at the base of the robot. In particular, the distance traveled on the circular trajectory was mapped to the lateral position of the vehicle. During the first tests, the vehicle was modeled to hover 5 m above the ground. During the second set of tests, it was constantly moved with 200 km/h at an altitude of 25 m and the visual motion was scaled up by a factor of 5.

#### Environment

The visual environment was modeled using the 3D rendering engine OGRE (Section 3.3). For both tests, the vehicle was placed in a forest scene with small hills of not more than 20 m in height. The ground was texturized with a noisy soil texture to provide rich visual feedback. On a square kilometer, in average 4000 trees were randomly placed and the initial starting position over the terrain varied for each flight.

Figure 4.1a shows the image displayed at the starting position during the first tests while Figure 4.1b shows the visualization at the beginning of a trail during the second series of tests.

#### Participants

Three males participated in this preliminary test. They had experience with flight simulation tasks on the CyberMotion simulator and thus where familiar with the dynamics. All subjects had normal or corrected to normal vision.

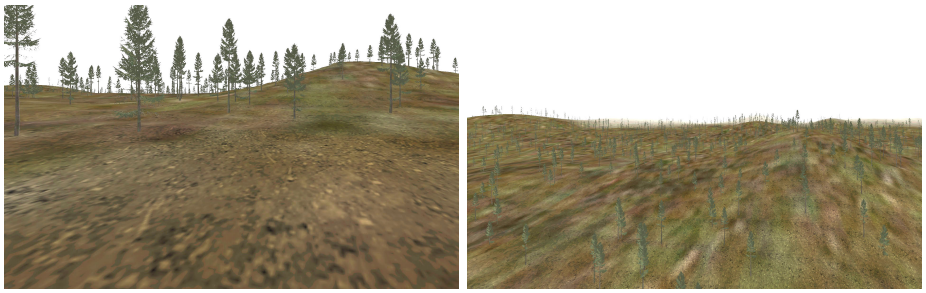

**Figure 4.1:** Visualization during (a) the first set of tests and (b) the second set of tests.

### 4.1.2 Design and Procedure

During the first set of tests, subjects were asked to hover as stable as possible close to the ground. The main task was therefore to counter control for lateral crosswinds.

After entering the simulator, participants were instructed with a brief training session. They performed once the task with 90° FoV to familiarize with the simulator motion and the experimental conditions.

Each participant carried out the flight task with two display settings: 1. screen with small FoV (45°) and 2. screen with wide FoV (90°). Both visual conditions were combined with three motion conditions to investigate the influence of motion feedback: 1. without physical motion; 2. full motion feedback and 3. disturbed motion feedback. The vertical FoV was 45° in all conditions.

The vehicle was affected by lateral cross winds that could be perceived both visually and vestibularly. The cross winds acted directly on the control input signal as a disturbance and were randomly generated. The disturbance signal was computed once and used for all flights to maintain comparability. It could reach up to a factor of 0.3 of the input signal.

Physically inaccurate motion due to motion cueing was simulated by introducing a disturbing roll motion of up to 25° on axis 6. This precomputed random motion was not related to the task. To accommodate to the next condition, the first 10 s of the simulation had neither wind nor physical motion disturbance.

Only short preliminary tests were run. The subjects performed three blocks each. A block consisted of three conditions (no motion, 45° and 90°) repeated four times in random order. Short breaks after four slaloms were allowed to prevent motion sickness. An entire session lasted approximately one hour.

### 4.1.3 Measures

Driver's performance was measured in terms of lateral deviation. The root mean square error was computed from the distance to the initial central position, averaged and compared between the tested conditions. All data was recorded at the rate of 12 ms for the entire experiment.

### 4.1.4 Results

For the first series of tests, data was not evaluated. Subjects reported that they were able to recognize lateral motion only by monitoring single pixels on the screen. Results showed similar

root mean square errors for all conditions and thus underline the subjects' statements.

With the second setup, we found an increase of pilots' performance when physical motion was simulated. This effect was statistically significant although no conclusion should be drawn since only three subjects participated in this preliminary experiment. Additional disturbance on the motion did not influence the pilot. Furthermore, no improved control performance could be observed with a FoV of 90° compared to 45° in any of the motion conditions (Figure 4.2).

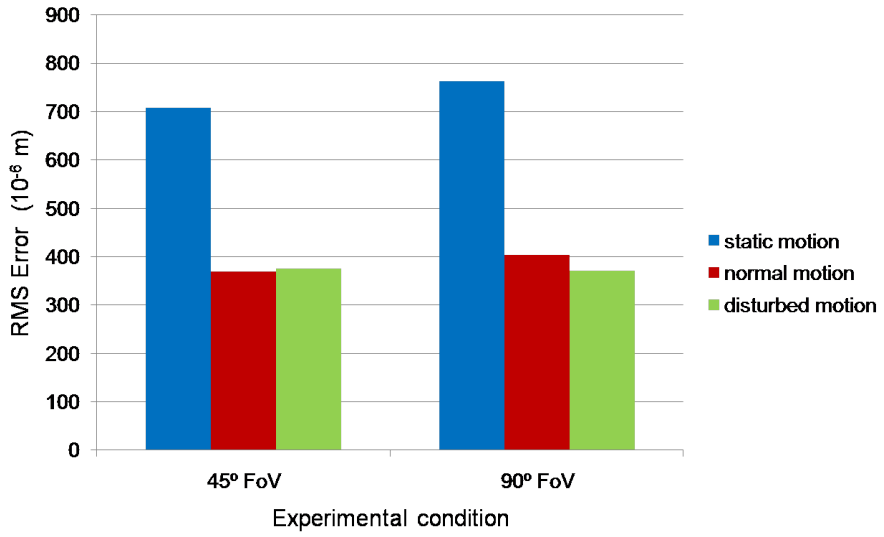


**Figure 4.2:** Root mean square error of the second flight control experiment on straight flight under different visual and motion feedback conditions.

### 4.1.5 Discussion

Our tests suggest that motion feedback in general has a positive influence on the performance of a pilot while an effect of the size of the FoV is not measurable. This finding revealed that small disturbances in the vestibular perception are tolerated by the human brain.

The main finding is consistent with previous work [Nieuwenhuizen et al., 2009]. However, it turned out that the addressed problem was not well posed and we were therefore unable to find sufficient results. A positive effect of a wide FoV achieved through the xSight HMD cannot be expected. It can be assumed, based on verbal reports of the subjects and objective measurements, that at least low order flight stabilization control tasks can be performed with a small FoV as long as environmental cues are present [Patterson et al., 2006].

Therefore, we decided to move on to driving simulation. In ground based navigation, it is not possible to focus on very distant objects and use them as reference. In order to drive precisely, it is important to rely more on local optical flow rather than point tracking. Therefore, the FoV could become more relevant.

## 4.2 Experiment on Driving Simulation

It is well known that large projection screens with a wide FoV provide motion cues in the periphery of the visual field that can result in a greater sense of vection [Hettinger and Riccio, 1992], [Mohler et al., 2005], more accurate navigation abilities [Alfano and Michel, 1990], and more accurate perception of self-motion [Pretto et al., 2009]. For instance, in a driving simulation scenario, a wide FoV provides a better estimation of speed [Jamson, 2000; Pretto et al., 2008] while in flight simulation a FoV bigger than 60° helps in the cruise phase [Keller et al., 2003]. However, motion-based simulators often lack the space for large projection screens, and therefore small screens or HMDs are sometimes used.

Traditional HMDs provide a small FoV and create discomfort in the user [Mon-Williams et al., 1993]. Wide FoV visualization systems may also result in greater simulator sickness compared with more limited FoV devices [Sparto et al., 2004]. However, recent lightweight HMDs, combined with head tracking, reduce the users' discomfort and provide a wide horizontal FoV [Peli, 1998]. Yet, these devices influence distance judgments [Willemsen et al., 2009]. Therefore, the use of HMDs instead of large screens, and the corresponding impacts on driving capabilities, is still an issue but also represents an interesting option for motion-based driving simulators. Moreover, the effects on driving performance of a wide FoV in these two types of visualization devices need to be assessed using state-of-the-art setups. To address these issues we used our CyberMotion simulator to compare drivers' performance on a slalom task with different visualization setups and different FoV sizes. Such task was chosen because it requires driving accuracy, which might be influenced by the visual information available from wide FoVs.

Simulated motion represents also an important factor in driving precision and, depending on the visualization device, this might interfere with the drivers' accuracy. Specifically in absence of head tracking, the HMD could create visuo/vestibular conflict due to unintentional head motion induced by the simulator motion. Therefore, we compared drivers' performance also between static conditions in which head motion is minimized.

### 4.2.1 Experimental Setup

#### Apparatus

For this study the CyberMotion Simulator was equipped with the force feedback steering wheel for closed-loop control of the virtual car. As visualization devices, we used the existing projection system with a horizontal FoV of 90° and a vertical FoV of 45° (Figure 4.3a) and tested it against the Sensics xSight 6123 HMD with a horizontal FoV of up to 118° and a vertical FoV of 45° (Figure 4.3b).

#### Vehicle Simulation

Heading and roll motion of the virtual car were simulated according to a simple vehicle model based on Ackermann steering geometry, using axis 5 and 6 respectively (Figure 4.4). No motion filters were implemented in order to ensure a minimal delay between driver's input and the reaction of the simulator. Lateral translations were mapped into planar circular trajectories with a radius of 3.1 m. The lateral displacement on the road was simulated by rotating axis 1 at

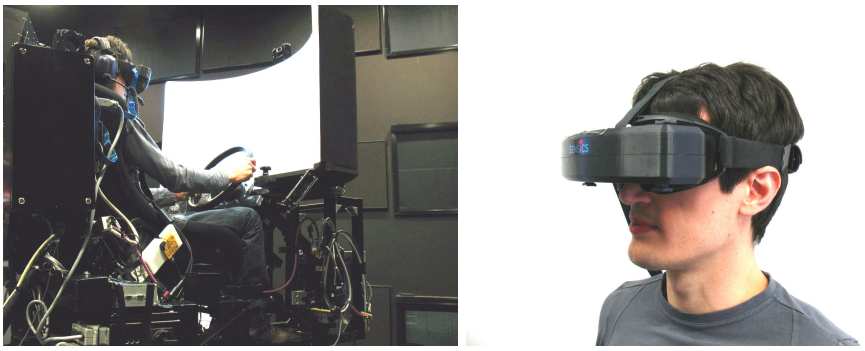

**Figure 4.3:** (a) The projection screen mounted to the CyberMotion Simulator; (b) the Sensics xSight 6123 HMD.

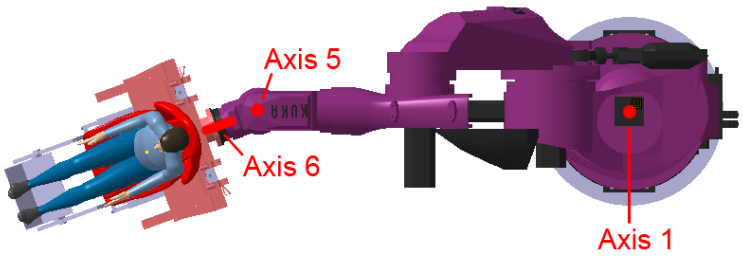


**Figure 4.4:** A sketch of the simulator axis used in the experiment, seen from the top. Axis 1 at the base simulated lateral motion. Heading and roll motions were simulated by axis 5 and 6.

the base of the robot. In particular, the distance traveled on the circular trajectory was mapped to the lateral position of the car on the road with a scale factor of 0.6 [Pretto et al., 2009].

### Visual Environment

The visual environment was modeled using the 3D rendering engine OGRE (Section 3.3) and consisted of a straight road in a forest setting. Trees of different size were placed randomly alongside the road and were repositioned throughout the experiment. A stone wall flanked the textured road to provide a richer visual feedback (Figure 4.5).

The slalom path was outlined by 15 gates over three consecutive sections. Each gate was 2 m wide and alternately displaced 3 m to the left and to the right of the center line on a two-lane road. The distance between gates was 62.5 m in the first and third section, while it varied between 45 m and 55 m, in steps of 2.5 m, in the middle section. At every run, all five inter-gate distances in the middle section occurred only once, in random order.

### Participants

Ten experienced drivers (1 female, 9 males) participated in the experiment. They had at least four years of driving experience on a daily basis. The age of the participants was ranging from 22 to 38 with an average of 25.7 years. All subjects had normal or corrected to normal vision. None of them wore glasses. Before entering the simulator they signed an informed consensus.

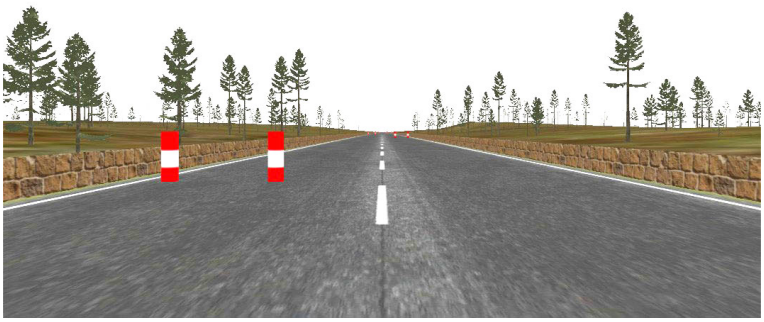

**Figure 4.5:** Screenshot of the environment as displayed on the screen with an horizontal FoV of 90° and a vertical FoV of 45°.

### 4.2.2 Design and Procedure

The drivers' task was to complete the slalom course and drive as smoothly as possible through each gate. Participants were instructed to rest their head at the back of the seat to minimize involuntary head movements. The simulation started 100 m before the first gate in the middle of the road and lasted for another 100 m after the last gate.

After entering the simulator, participants were provided with a brief training session. First, they saw a video of the optimal driving path; afterwards, they performed once the slalom with the screen setup and 90° FoV to familiarize with the simulator motion and the experimental conditions. The virtual vehicle was traveling at a constant speed of 70 km/h.

Each participant carried out the slalom maneuver with five display settings: 1. screen with small FoV (45°); 2. HMD with small FoV (45°); 3. screen with wide FoV (90°); 4. HMD with wide FoV (90°); 5. HMD with very wide FoV (118°). Two additional conditions without physical motion (screen and HMD with 90° FoV) to control for HMD discomfort with static head were added. The vertical FoV was 45° in all conditions.

In a typical driving session, a driver performed four blocks of twelve slalom maneuvers, alternating with another driver after each block. The visualization devices were alternated over the four blocks and between the two drivers. A block with HMD consisted of four conditions (no motion, 45°, 90° and 118°) repeated three times in random order. In turn, a block with screen consisted of three conditions (no motion, 45° and 90°) repeated four times in random order. Short breaks after four slaloms were allowed to prevent motion sickness. An entire session lasted approximately four hours.

### 4.2.3 Measures

A smooth trajectory that passes through the center of each gate was computed using cubic Hermite splines as a flexible approximation of a sinusoid curve. Driver's performance was measured in terms of deviation from this path within each two consecutive gates. The root mean square error from the path was averaged across participants and compared between the tested conditions.

All data was recorded at the rate of 12 ms for the entire experiment. The data from the first

and the last gate, as well as from missed gates, were excluded from the analysis.

### 4.2.4 Results

We found a significant difference in the performance between the two devices (Subsection 1.1.4). At a paired-sample t-test the HMD resulted to provide significantly worse results than the screen ($t9 = 3.566$, $p < 0.01$). This result is supported by the observation that 27 gates were missed when using the HMD, while only one was missed when using the screen. The size of the FoV had no significant effect on driving precision, with both HMD ($F(2, 18) = 0.85$, $p = 0.41$) and screen ($t9 = 0.593$, $p = 0.568$) (Figure 4.6). Simulated motion did not improve driver's performance in our slalom task ($F(1, 9) = 0.17$, $p = 0.69$). Furthermore, there was no interaction between motion and the two devices ($F(1, 9) = 0.99$, $p = 0.35$).

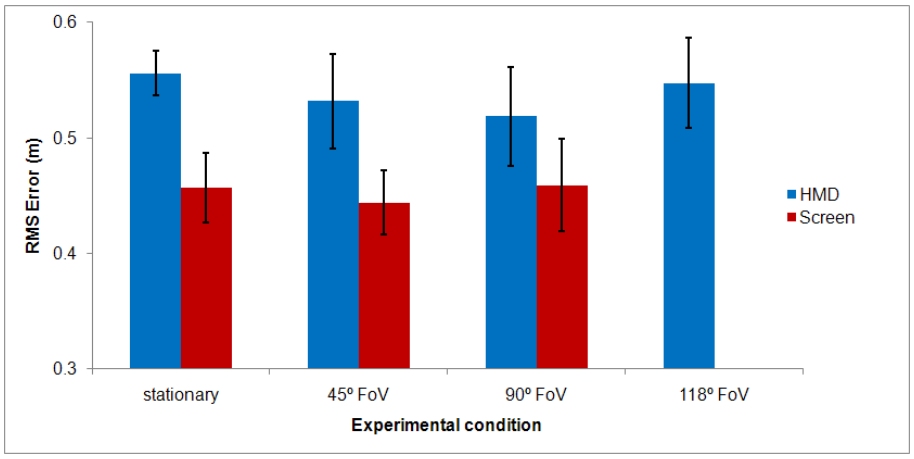


**Figure 4.6:** Driving performance under different display and motion conditions. Each bar represents data averaged across 10 subjects. The conditions with a stationary simulator were provided with a FoV of 90°. The error bars indicate standard errors.

### 4.2.5 Discussion

Our study shows that the deviation from the optimal path in a slalom-driving task is lower when drivers see the virtual environment on a screen rather than on an HMD. This result is consistent with the findings of a previous study in which subjects performed worse with HMD on a self-motion perceptual task [Riecke et al., 2005]. Although the resolution, as well as brightness and contrast, were superior in the HMD as compared to the screen, other features of the device might have contributed to its bad performance. A recent study compared HMDs with real world situations and showed that restricted FoV together with high inertial weight on the head results in bad distance judgments [Willemsen et al., 2009]. However, in our study the HMD had a lower weight and a wider FoV, therefore we might assume that potential effects on perception were reduced.

Other critical factors of the HMD are pincushion and keystone distortion. It has been shown that pincushion distortion does not affect perceptual judgments [Kuhl et al., 2008]. In the Sensics HMD, however, the image of each eye is generated by merging the images of six sub-displays,

each of them with little pincushion distortion. Moreover, no method to compensate for keystone distortions in the individual displays is provided by the manufacturer and, therefore, it is not possible to set up a perfect transition between the sub-displays in the outer regions of the visual field. How all these optical distortions are perceived is still an issue that needs to be further investigated.

Recent works have shown that a FoV limited to 58° and 42° did not affect humans' abilities in distance judgments [Creem-Regehr et al., 2005; Knapp and Loomis, 2003]. In line with this, our study demonstrates that a large FoV does not improve drivers' capabilities to accomplish a slalom task. This result can be explained by the drivers' gaze behavior when driving around a curve. It has been shown, indeed, that drivers look at the inner edge of the road when approaching a curve [Land and Lee, 1994] and therefore, in a slalom task, the driver's gaze is likely to be directed towards the inner side of the approaching gate. In our experiment, the widest visual angle between the heading of the vehicle and the approaching gate was less than 10°. This would indicate that the slalom task is essentially performed in central vision, and additional cues provided by the periphery of the visual field are not taken into account. The smallest FoV condition (45°) of our experiment contained already all the useful information and a slalom path with sharper curves would be necessary to enhance the role of a wide FoV.

In our study physical motion did not affect drivers' performance. In contrast, it has been shown that physical motion improves pilot's performance on a complex helicopter control task [Nieuwenhuizen et al., 2009]. This suggests that motion supports the pilot to carry out demanding maneuvers, but it is less important when operating vehicles with more direct control as in our experiment. We assume that experienced drivers could easily carry out our slalom task, resulting in performance saturation. This should be addressed in future projects by increasing the difficulty of the task.

Finally, the lower performance in the HMD conditions cannot be attributed to the lack of head tracking. In fact, no interaction effect was found between trials with and without physical motion, even within the HMD conditions. This supports the assumption that unintentional head motion was limited and visual/vestibular conflicts were minimal.

# Chapter 5

# Conclusion

This thesis addressed the integration of the Sensics xSight 6123 HMD into a 3D environment and the installation on the CyberMotion simulator. The implementation included the design and realization of a robust communication interface for an easy integration into other experiments. After extensive testing, we designed several experiments to investigate the benefit of the HMD in typical simulation conditions compared to a curved projection screen. Our findings showed that the screen should be preferred over the HMD in almost all conditions.

For the integration of the xSight HMD, we decided to use the object oriented and free 3D engine OGRE. A new camera class for stereo setups with an asymmetric FoV was designed to hold three cameras (one for each eye and an additional scene camera for the experimenter), and can be integrated in existing and future experiments easily. The camera settings of the HMD with partial binocular overlap were derived through measurements since no documentation was available. In order to provide a uniform image across both eyes, the alignment of all sub-displays relative to each other as well as the color settings were calibrated.

The HMD system is composed of the HMD, a small belt pack, a control unit and the image generating vision PC was mounted on the CyberMotion simulator. To protect the fragile control unit from high accelerations, but still save on the expensive and prone to noise trunk cable for the connection to the belt pack, we secured it with a metal frame on the first axis in an upright orientation. The vision PC is located in the control room. Finally, we designed and implemented a protocol for the communication between the vision PC and the simulator.

In order to investigate the benefit of the HMD on humans' performance in a motion simulator task compared to the existing projection screen, we designed several experiments. The HMD has a better resolution and a wider FoV than the screen but might be uncomfortable to use. For preliminary tests, we first analyzed the influence of the FoV on flight control tasks with inaccurate motion feedback due to motion cueing. Since the HMD was not available, this experiment was conducted with the screen only and FoVs of 45° and 90°. For the physical motion, we cross-compared static, physically correct, and inaccurate motion feedback. The subjects were asked to stabilize a vehicle similar to an helicopter in the lateral domain and prevent drift. As a result we found a better performance of the pilots with simulated physical motion than with no motion. However, no measurable improvement through a large FoV could be shown. We suppose that the FoV does not play an important role in most flight tasks. In our experiments the subjects reported that they were able to stabilize the vehicle with just few environmental cues in the central FoV.

Consequently, we chose a driving simulation for the final experiment. We expected a large FoV to be more important in ground based navigation since the driver has to carefully focus on the surroundings of the car for a good driving performance. We implemented a slalom driving task with 15 gates alternating on the left and right side of a straight road in a rich forest environment. The subjects' task was to follow the path outlined by the gates as smooth as possible while the car was traveling with a constant speed of 70 km/h. In a randomized experiment, we tested viewing conditions with a FoV restricted to 45° and 90° with both the HMD as well as the screen, and additionally 118° only with the HMD. As the most important finding, we showed that subjects perform significantly worse with the HMD compared to the screen. However, it turned out that the FoV did not have an influence on the driving performance either. Therefore we suggest that humans perform most navigation tasks without the use of the peripheral regions of their FoV. This should be addressed in more detail by increasing the difficulty of the task in future work.

Since the screen led to better results and less motion sickness across all visual conditions, we suggest the use of a screen whenever possible. We assume that the bad performance with the HMD is caused by the lack of some important aspects of the calibration. The configuration maps the image of the flat displays onto a hemisphere surrounding the eye without corrections for keystone effects and pincushion distortion. This results in overlapping images in the outer regions of the FoV and potentially causes discomfort in the user. Without these limitations we would expect an improved performance.

However, in some situation when stereo vision is required and the device is only used for short times, the HMD could be an alternative solution. A simple setup without an extensive configuration and the portability makes it an interesting option for mobile simulators.

# Bibliography


Alfano, P. L. and G. F. Michel (1990). Restricting the field of view: perceptual and performance effects. *Perceptual & Motor Skills 70*(1), 35–45.

AMST Systemtechnik GmbH (2010). http://www.amst.co.at.

Axenfeld, T. and H. Pau (1992). *Lehrbuch der Augenheilkunde*. Elsevier.

Bortz, J. (2005). *Statistik für Human- und Sozialwissenschaftler* (6 ed.). Springer.

Bortz, J. and N. Döring (2006). *Forschungsmethoden und Evaluation für Human- und Sozialwissenschaftler* (4 ed.). Springer.

Cappel, K. L. (1967). Patent: Motion Simulator.

Creem-Regehr, S. H., P. Willemsen, A. A. Gooch, and W. B. Thompson (2005, Januar). The influence of restricted viewing conditions on egocentric distance perception: implications for real and virtual indoor environments. *Perception 34*(2), 191–204.

eMagin Corporation (2010). http://www.3dvisor.com.

Ferris, S. H. (1972). Motion parallax and absolute distance. *Journal of Experimental Psychology 95*(2), 258–263.

Forsyth, B. A. C. and K. E. MacLean (2006). Predictive Haptic Guidance: Intelligent User Assistance for the Control of Dynamic Tasks. *IEEE Transactions on Visualization and Computer Graphics 12*(1), 103–113.

Gibson, J. J. (1979). *The Ecological Approach to Visual Perception*. Houghton Mifflin.

Goldstein, E. B. (2002). *Sensation and Perception*. Wadsworth.

Gough, V. E. and S. G. Whitehall (1962). Universal tyre test machine. In *Proceedings of the 9th International Technical Congress F.I.S.I.T.A.*, pp. 117–135.

Grabe, V., P. Pretto, P. Rubuffo Giordano, and H. H. Bülthoff (2010). Influence of display type and field of view on drivers' performance in a motion-based driving simulator. In *Proceedings of the Driving Simulation Conference*, Paris, France.

Grant, P. R. and L. D. Reid (1997). Motion washout filter tuning : Rules and requirements. *Journal of aircraft 34*(2), 145–151.

Hettinger, L. J. and G. E. Riccio (1992). Visually induced motion sickness in virtual environments. *Presence: Teleoperators and Virtual Environments 1*(3), 306–310.

Hoppe, H. (1997). View-dependent refinement of progressive meshes. In *Proceedings of the 24th annual conference on computer graphics and interactive techniques*, New York, NY, USA, pp. 189–198.

Ishida, M., H. Fushiki, H. Nishida, and Y. Watanabe (2008). Self-motion perception during conflicting visual-vestibular acceleration. *Journal of vestibular research : equilibrium & orientation 18*(5-6), 267–272.

Jamson, H. (2000). Driving simulation validity: issues of field of view and resolution. In *Proceedings of the Driving Simulation Conference*, Paris, France, pp. 57–64.

Kandel, E. R., J. H. Schwartz, and T. M. Jessell (2000). *Principles of Neural Science* (4 ed.). McGraw-Hill.

Keller, M., T. Schnell, K. Lemos, L. Glaab, and R. Parrish (2003). Pilot performance as a function of display resolution and field of view in a simulated terrain following flight task using a synthetic vision system. In *Digital Avionics Systems Conference*, pp. 9.E.591–12.

Kennedy, R. S., N. E. Lane, K. S. Berbaum, and M. G. Lilienthal (1993). Simulator Sickness Questionnaire: An Enhanced Method for Quantifying Simulator Sickness. *The International Journal of Aviation Psychology 3*(3), 203–220.

Knapp, J. M. and J. M. Loomis (2003). Limited Field of View of Head-Mounted Displays Is Not the Cause of Distance Underestimation in Virtual. *Presence: Teleoperators and Virtual Environments 13*(5), 572–577.

Kuhl, S. A., W. B. Thompson, and S. H. Creem-regehr (2008). HMD calibration and its effects on distance judgments. In *Proceedings of the 5th Symposium on Applied Perception in Graphics and Visualization*, Number August, Los Angeles, USA, pp. 15–22.

Kuka AG (2010). http://www.kuka-entertainment.com/en/.

L-3 Communications Link Simulation & Training (2010). http://www.link.com.

Land, M. F. and D. N. Lee (1994). Where we look when we steer. *Nature 369*(6483), 742–744.

Lewis, J. L., M. B. Carroll, R. H. Morales, and T. D. Le (2002). Patent: Androgynous, reconfigurable closed loop feedback controlled low impact docking system with load sensing electromagnetic capture ring.

Link Jr., E. A. (1931). Patent: Combination training device for student aviators and entertainment apparatus.

Luebke, D. and C. Erikson (1997). View-Dependent Simplification Of Arbitrary Polygonal Environments. In *Proceedings of the 24th annual conference on Computer graphics and interactive techniques*, New York, NY, USA, pp. 199–208.

Mohler, B. J., B. E. Riecke, W. B. Thompson, and H. H. Bülthoff (2005). Measuring vection in a large screen virtual environment. In *Proceedings of the 2nd Symposium on Applied Perception in Graphics and Visualization*, A Coroña, Spain, pp. 103–109.

Mon-Williams, M., J. P. Warm, and S. Rushton (1993). Binocular vision in a virtual world: visual deficits following the wearing of a head-mounted display. *Ophthalmic and Physiological Optics 13*(4), 387–391.

Nahon, M. A. and L. D. Reid (1990). Simulator Motion-Drive Algorithms: A Designer's Perspective. *Journal of Guidance Control and Dynamics 13*(2), 356–362.

National Aeronautics and Space Administration (NASA) (2010). http://www.nasa.gov.

NaturalPoint Inc. (2010). http://www.naturalpoint.com/trackir/.

Nieuwenhuizen, F. M., P. M. T. Zaal, H. J. Teufel, M. Mulder, and H. H. Bülthoff (2009). The Effect of Simulator Motion on Pilot Control Behaviour for Agile and Inert Helicopter Dynamics. In *Proceedings of the 35th European Rotorcraft Forum*, Hamburg, Germany, pp. 1–13.

NVIS Inc. (2010). http://www.nvisinc.com.

Patterson, R., G. A. Geri, B. P. Dyre, B. J. Pierce, S. C. Akhtar, C. M. Covas, and W. Morgan (2006). Active heading control in simulated flight based on vertically extended contours. *Perception & psychophysics 68*(4), 593–600.

Peli, E. (1998). The visual effects of head-mounted display (HMD) are not distinguishable from those of desk-top computer display. *Vision Research 38*(13), 2053–2066.

Pretto, P., H.-G. Nusseck, H. Teufel, and H. H. Bülthoff (2009). Effect of lateral motion on drivers performance in the MPI motion simulator. In *Proceedings of the Driving Simulation Conference*, Monaco, pp. 121–131.

Pretto, P., M. Ogier, H. H. Bülthoff, and J.-P. Bresciani (2009). Influence of the size of the field of view on motion perception. *Computers & Graphics 33*(2), 139–146.

Pretto, P., M. Vidal, and A. Chatziastros (2008). Why fog increases the perceived speed. In *Proceedings of the Driving Simulation Conference*, Monaco, pp. 223–235.

Reason, J. T. (1978). Motion sickness adaptation: a neural mismatch model. *Journal of the Royal Society of Medicine 71*(11), 819–829.

Riecke, B. E., J. Schulte-Pelkum, and H. H. Bülthoff (2005). Perceiving Simulated Ego-Motions in Virtual Reality - Comparing Large Screen Displays with HMDs. In *Proceedings of the International Society for Optical Engineering*, San Jose, USA, pp. 344–355.

Robuffo Giordano, P., H. Deusch, J. Lächele, and H. H. Bülthoff (2010). Visual-Vestibular Feedback for Enhanced Situational Awareness in Teleoperation of UAVs. In *Proceedings of the AHS 66th Annual Forum and Technology Display*, Phoenix, AZ, USA, pp. 1–10.

Robuffo Giordano, P., C. Masone, J. Tesch, M. Breidt, L. Pollini, and H. H. Bülthoff (2010). A Novel Framework for Closed-Loop Robotic Motion Simulation - Part II : Motion Cueing Design and Experimental Validation. In *Proceedings of the 2010 IEEE International Conference on Robotics and Automation*, Anchorage, AK, USA, pp. 3896–3903.

Roza, M., M. Wentink, and P. Feenstra (2007). Performance Testing of the Desdemona Motion System. In *Proceedings of AIAA Modeling and Simulation Technologies Conference and Exhibit*, Number August, Hilton Head, SC, USA, pp. 1–14. American Institute of Aeronautics and Astronautics.

Sensics Inc. (2010). http://sensics.com/products/xSight/.

Sensodrive GmbH (2010). http://sensodrive.de.

Sövényi, S. and R. B. Gillespie (2007). Cancellation of Biodynamic Feedthrough in Vehicle Control Tasks. *IEEE Transactions on Control Systems Technology 15*(6), 1018–1029.

Sparto, P. J., S. L. Whitney, L. F. Hodges, J. M. Furman, and M. S. Redfern (2004). Simulator sickness when performing gaze shifts within a wide field of view optic flow environment: preliminary evidence for using virtual reality in vestibular rehabilitation. *Journal of Neuro-Engineering and Rehabilitation 1*(14).

Steele, M. and R. B. Gillespie (1994). Shared Control between Human and Machine: Using a Haptic Steering Wheel to Aid in Land Vehicle Guidance. In *Human Factors and Ergonomics Society Annual Meeting Proceedings: Surface Transportation*, pp. 1671–1675.

Stewart, D. (1965). A platform with six degrees of freedom. *Proceedings of the Institute of Mechanical Engineering 180*(1), 371–386.

Terzibas, C. (2010). http://sourceforge.net/projects/xdevl/.

Teufel, H. J., H.-G. Nusseck, K. A. Beykirch, J. S. Butler, M. Kerger, and H. H. Bülthoff (2007). MPI Motion Simulator: Development and Analysis of a Novel Motion Simulator. In *Proceedings of the AIAA Modeling and Simulation Technologies Conference and Exhibit*, Reston, VA, USA, pp. 1–11.

Torus Knot Software Ltd. (2010). http://www.ogre3d.org.

Toyota Motor Corporation (2010). http://www.toyota-future.com.

Treisman, M. (1977). Motion sickness: an evolutionary hypothesis. *Science 197*(4302), 493–495.

Wagner, C. R., N. Stylopoulos, P. G. Jackson, and R. D. Howe (2007). The Benefit of Force Feedback in Surgery : Examination of Blunt Dissection. *Presence: Teleoperators and Virtual Environments 16*(3), 252–262.

Westheimer, G. (2009). Visual acuity: information theory, retinal image structure and resolution thresholds. *Progress in Retinal and Eye Research 28*(3), 178–186.

Willemsen, P., M. B. Colton, S. H. Creem-Regehr, and W. B. Thompson (2009). The effects of head-mounted display mechanical properties and field of view on distance judgments in virtual environments. *ACM Transactions on Applied Perception 6*(2), 1–14.

Wright, W. G., P. DiZio, and J. R. Lackner (2005). Vertical linear self-motion perception during visual and inertial motion: More than weighted summation of sensory inputs. *Journal of vestibular research : equilibrium & orientation 15*(4), 185–195.

Xia, J. C. and A. Varshney (1996). Dynamic View-Dependent Simplification for Polygonal Models. In *Proceedings of the 7th conference on Visualization*, San Francisco, CA, USA, pp. 327–334.

# Selbständigkeitserklärung

Hiermit versichere ich, dass ich die vorliegende Diplomarbeit selbständig und nur mit den angegebenen Hilfsmitteln angefertigt habe und dass alle Stellen, die dem Wortlaut nach anderen Werken entnommen sind, durch Angaben von Quellen als Entlehnung kenntlich gemacht worden sind. Diese Diplomarbeit wurde in gleicher oder ähnlicher Form in keinem anderen Studiengang als Prüfungsleistung vorgelegt.

Ort, Datum Unterschrift